Counteractive effects of regional transport and emissions control on the formation of fine particles: a case study during the Hangzhou G20 Summit

Ying Ji[1], Xiaofei Qin[1], Bo Wang[1], Jian Xu[1], Jiandong Shen[3], Jianmin Chen[1], Kan Huang[1,2,4,*], Congrui Deng[1,2,*], Renchang Yan[3], Kaier Xu[3], Tian Zhang[3]

[1]Shanghai Key Laboratory of Atmospheric Particle Pollution and Prevention (LAP3), Department of Environmental Science and Engineering, Fudan University, Shanghai 200433, China
[2]Shanghai Institute of Eco-Chongming (SIEC), No.3663 Northern Zhongshan Road, Shanghai 200062, China
[3]Hangzhou Environmental Monitoring Center, Hangzhou, Zhejiang 310007, China
[4]Institute of Atmospheric Sciences, Fudan University, Shanghai 200433, China

Correspondence to: K. Huang (huangkan@fudan.edu.cn); C. R. Deng (congruideng@fudan.edu.cn)

Abstract. To evaluate the effect of temporary emissions control measures on air quality during the 2016 G20 Summit held in Hangzhou, China, an intensive field campaign was conducted with focus on aerosol chemistry and gaseous precursors from 15 August to 12 September, 2016. The concentrations of fine particles were reduced during the intense emission control stages, of which the reduction of carbonaceous matters was mostly responsible. This was mainly ascribed to the decreases of secondary organic aerosols via the suppression of daytime peak SOC formation. Although the regional joint control was enacted extending to the Yangtze River Delta region, the effect of long-range transport on the air quality of Hangzhou was ubiquitous. Unexpectedly high NOx concentrations were observed during the control stage when the strictest restriction on vehicles was implemented, owing to the contributions from upstream populous regions such as Jiangsu and Shandong provinces. In addition, the continental outflow travelling over the ocean triggered a short pollution episode on the first day of the G20 Summit, resulting in a significant enhancement of the nitrogen/sulfur oxidation rates. After the Summit, all the air pollutants evidently rebounded with the lifting of various control measures. Overall, the fraction of secondary inorganic aerosols (SNA) in $PM_{2.5}$ increased as relative humidity increased, but not for the concentrations of $PM_{2.5}$. Aerosol components that had distinctly different sources and formation mechanisms, e.g. sulfate/nitrate and elemental carbon, showed strong correlations

exclusively during the regional/long-range transport episodes. The SNA/EC ratios, which was used as a proxy for assessing the extent of secondary inorganic aerosol formation, were found significantly enhanced under transport conditions from northern China. This study highlighted that the emission control strategies were beneficial for curbing the particulate pollution whereas the regional/long-range transport may offset the local emission control effects to some extent.

1 Introduction

Fine particulate matters (PM) are associated with air quality, public health, and the Earth's climate (Garrett and Zhao, 2006;Liao et al., 2006;Menon et al., 2008;Tie and Cao, 2009;Kim et al., 2008). China, especially its megacities, has experienced frequent and severe air pollutions during the past decade. Severe air pollution episodes were often accompanied with high PM levels. The chemical compositions of PM mainly consist of secondary inorganic aerosols (SIA) and organic matters (OM) that can be differentiated into the primary organic aerosol (POA) and secondary organic aerosol (SOA). SIA typically accounted for 40-50 % of the particulate masses during heavy pollution events and OM of 30-40 % (Sun et al., 2016;Chen et al., 2015;Huang et al., 2012;Guo et al., 2014). During a historical regional pollution episode, the mass ratio of SIA was over 1/3 at both megacities (Beijing and Shanghai) and the remote region (Huaniao Isle over the East China Sea) (Wang et al., 2015a).

After the holding of the 2008 Olympic Games and 2014 APEC (Asia-Pacific Economic Cooperation) Summit in Beijing, the G20 Summit (Group of Twenty Finance Ministers and Central Bank Governors) in Hangzhou from 4 to 6 September 2016 was the biggest international event in China in recent years. It is an international economic cooperation forum aiming at promoting open and constructive discussions and research on substantive issues between developed and emerging market countries in order to seek cooperation and promote international financial stability and economic sustainability. To improve the air quality during the Summit, the government took strict control measures to reduce air pollutant emissions from transportation, industry, construction sites, and power plants. Thus, it is an excellent opportunity to conduct impact assessment of control measures on the atmospheric components. In addition, this assessment is expected to deduce the sources of different air pollution components and provide references for the prevention and control of air pollution in the future.

The components of air pollutants are affected by both emission sources and weather conditions (Wang and Dai, 2016;Liu et al., 2016a;Schleicher et al., 2012). During the 2008 Olympic Games and the 2014 APEC Summit, similar control measures were taken in Beijing and surrounding areas to achieve a good status of air quality. During the 2008 Beijing Olympics, the decrease of $PM_{2.5}$ mass was mainly due to the reduction of SIA, and the unexpected $PM_{2.5}$ increase during the emission control period may be related to poor weather conditions such as transport from the south and a small amount of precipitation (Li et al., 2013). In addition, the contribution of SIA increased while opposite for organics during the haze development, indicating that NOx emission control should be a priority for improving air quality in Chinese mega-cities (Pan et al., 2016). Particulate matters and street dust remained high through the Olympic period probably due to redistribution of existing sources, implying that the aim of zero pollution is not achievable in the short term (Qiao et al., 2016). Moreover, significant reductions of NO_X and VOCs were observed in the first two weeks after the control measures were fully implemented. However, the levels of ozone, sulfate and nitrate in $PM_{2.5}$ increased and high levels of ozone may accelerate the oxidation of SO_2 to form sulfate (Wang et al., 2010). During the 2014 APEC Summit, all the aerosol components were significantly reduced while the O_3 concentration was still high (Wang et al., 2015b). Reductions of the precursors of secondary aerosols over regional scales were crucial and effective in mitigating PM pollution (Sun et al., 2016;Chen et al., 2015). From the perspective of remote sensing, the regional emission control strategy could significantly lower the extent of regional transport (Huang et al., 2015). When the local emission reduction was weakened, the variability of weather condition would play a more important role and the regional long-range transport became important (Xu et al., 2016). Therefore, the mechanism of the control measures and meteorological conditions on perturbing the levels of air pollutants are complex.

The formation mechanisms of severe pollution are complex and have not been clarified so far, as well as the formations of nitrate and sulfate. The formation of nitrate is generally dominated by three pathways. Under the ammonia-rich conditions, nitrate is formed mainly via the reactions of gaseous HNO_3 or nitric acid in droplets; while in ammonia-poor environments, heterogeneous hydrolysis of N_2O_5 on aerosol surfaces dominated (Schryer, 1982;Pathak et al., 2009;Russell et al., 1986;Richards, 1983) and this pathway primarily occurs at night with high RH and low temperature (Lin et al., 2006). In the daytime, NOx reacted with hydroxyl radicals to produce nitric and nitrous acids via complex photochemical reactions (Khoder, 2002). As for sulfate, the gas-phase oxidation of SO_2 by OH radical

is the main pathway of its formation, and the heterogeneous uptake of SO_2 on pre-existing particles or in cloud droplets with oxidation by H_2O_2, O_3, NO_2 and metal ions is also important to form sulfate (Cheng et al., 2016;He et al., 2014;Khoder, 2002;Sander and Seinfeld, 1976). Both gas-phase and heterogeneous reactions are found responsible for the increase of fine particles, ultimately leading to the occurrence of haze (Li et al., 2013;Pan et al., 2016;Wang et al., 2010). The secondary formation of SIA was found to be related to heterogeneous aqueous reactions and was largely dependent on the ambient humidity (Wang et al., 2012). Humidity plays a more important role in the rapid increase of nitrate than that of sulfate and ammonium in $PM_{2.5}$ (Pan et al., 2016). The nitrate to sulfate ratios also exhibited dependence on relative humidity (RH) and the daily variation of $PM_{2.5}$ tracked the pattern of RH in Beijing (Cheng et al., 2014).

Air pollution has become serious in the Yangtze River Delta region because of the fast development of urbanization and industrialization over the past few years. Hangzhou is one of the major cities in the Yangtze River Delta, a large number of economic activities have made its air pollution increasingly prominent. Although some air pollution control measures have been adopted in recent years and the overall air quality in Hangzhou has been improved, air pollution incidents still occurred frequently. The average mass concentration of $PM_{2.5}$ were 118 μg m^{-3} during a haze period and the contribution of SIA species to $PM_{2.5}$ mass increased to almost 50% under haze and fog conditions in Hangzhou (Jansen et al., 2014). Iron/steel manufacturing and secondary aerosol were the main sources for fine particles (Liu et al., 2015a). In addition to the local emissions, it is also found that air mass pathways and cross-border transports controlled high $PM_{2.5}$ concentrations and formation in Hangzhou (Yu et al., 2014). The $PM_{2.5}$ and ozone levels in Hangzhou during the G20 Summit were considerably lower than previous by using the WRF-CMAQ modeling system (Li et al., 2017b).

In this study, meteorological parameters, gaseous precursors, and aerosol chemical components in Hangzhou before, during, and after the 2016 G20 Summit were analyzed. Learning how the emission control measures affected the chemical compositions, sources, and formation mechanisms of fine particles under variable meteorological conditions during the control periods can systematically evaluate the effectiveness of control measures and provide relevant basis for the improvement of environmental quality. Although studies about the impact of emissions control on air quality have been widely studied, there are some new findings in this study. Obvious increases of air pollutants even appeared during the two most rigorous control stages, the regional and long-range transport had

significant impact on the air quality of Hangzhou. The formation mechanism of sulfate was different from nitrate with the dominance of photochemical formation for sulfate but heterogeneous formation for nitrate. The implementation of emission control measures had a significant impact on modifying the diurnal patterns of SOC.

2 Methodology

2.1 Observational site

The observational site (120.17° N, 30.29° E) in this study is on the roof (~ 20 m high) of a residential building in Hangzhou, Zhejiang province. It is about 13 km from Hangzhou International Expo Center, which is the main venue of the G20 Summit (Fig. 1). This site is surrounded by the residential buildings in the north, south and east direction, and by several hospitals, with banks and convenience stores in the west. It is representative of mixed emissions such as residential, traffic, etc. During the study period, three zones with different emission control intensities were generally set up as shown in Fig. 1

2.2 Instrumentation

2.2.1 Water-soluble ions

Water-soluble components of airborne fine particles were continuously measured by an Ambient Ion Monitor (URG-AIM9000D) during the entire study period. The system consists of the Steam Jet Aerosol Collector (SJAC) and Ion Chromatography (ICS-2100, Dionex). Air flowed into the sampling tube at a rate of 16.7 L min^{-1}. The sampling tube is equipped with a $PM_{2.5}$ cyclone cutting head, which can separate out the particulate matters less than 2.5 microns in aerodynamic diameter. Part of the air passed through a liquid diffusion denuder at the rate of 3 L min^{-1} in order to remove the interfering gases (mainly SO_2 and HNO_3) and the rest of air was emptied. The air then mixed with the hot saturated water after entering the steam generator and the mixing chamber, turning aerosol particles to grow into droplets. The enlarged particles were separated by an inertial separator. After filtering, the aerosolized liquid was temporarily stored in an aerosol sample collector. Until the analysis time, the

collector automatically injected the samples into the ion chromatograph. The aerosolized water-soluble ions collected on-line were measured by two ion chromatographs through three-way device simultaneously.

The routine QA/QC included that all standard solutions were of excellent grade purity and re-prepared monthly. The correlation coefficients (R^2) of the standard curve were greater than 99.9 %, excepting for NH_4^+ of R^2>99.5 %. The flow rate of the AIM system was checked periodically and kept at 3 L min^{-1}.

2.2.2 OC/EC

Organic carbon (OC) and element carbon (EC) in $PM_{2.5}$ were measured using a Semi-Continuous OC/EC analyzer (SUNSET Laboratory). Particles with an aerodynamic particle diameter less than 2.5 μm were collected by the cyclone separator at a sampling flow rate of 8 L min^{-1} and the sampling time was 40 min per cycle. Air particles were collected on a circular quartz filter with a diameter of about 1.6 cm and an effective sampling area of 2.0 cm^2. The volatile organic compounds (VOCs) were removed by a multi-layer parallel organic denuder during sampling. After finishing the collection, we used the high purity helium gas to purge pipeline of the system, then the NIOSH (National Institute for Occupational Safety and Health) 5040 TOT (thermal-optical transmittance) was used for analysis within the duration of 15 ~ 20 min. The carbonaceous matters collected on the quartz film were gradually pyrolyzed and catalytically oxidized to CO_2 by the programmed temperature and thermo-optical method, and then quantified by a non-dispersive infrared detector (NDIR). The temporal resolution of measurement was 1 h and the OC/EC detect sensitivity (calculate as C) can reach 0.1μg m^{-3}. The instrument was calibrated with methane standard gas for each monitoring cycle and the monthly standard sucrose solution was used to calibrate methane standard gas.

2.2.3 $PM_{2.5}$ and trace gases

$PM_{2.5}$ was measured by a continuous particulate matter monitor (5030, Thermo, USA). A 43i SO_2 gas analyzer and a 42i NO-NO_2-NOx analyzer were used to measure the concentrations of trace gases.

2.2.4 Meteorological parameters

The meteorological parameters (wind speed, wind direction, relative humidity, temperature, and radiation) during the G20 period were all measured at the observational site. The height of the boundary layer was estimated based on a co-located aerosol lidar. It was determined based on the height where the decreasing rate of aerosol extinction coefficient was the most abrupt.

2.3 Data Analysis

2.3.1. Air mass back trajectory

The HYSPLIT (HYbrid Single-Particle Lagrangian Integrated Trajectory) model is a complete system for calculating simple air mass backward trajectories to dispersion and complex deposition simulations (Draxler and Rolph, 2012). To clarify the possible sources of various air pollutants, the hybrid single-particle Lagrangian integrated trajectory HYSPLIT4 was run online at the NOAA ARL READY Website (HYSPLIT4, 1997) using the meteorological data archives of Air Resource Laboratory (ARL). The meteorological input data used in the model was obtained from NCEP's global data assimilation system (GDAS) with a horizontal resolution of 0.5° × 0.5°. In this study, all back trajectories were calculated at 500m AGL (above ground level).

2.3.2. Concentration Weighted Trajectory (CWT) analysis

The concentration weighted trajectory (CWT) analysis (Hsu et al., 2003), a useful tool for source identification, was performed to pinpoint the potential geographic source regions of air pollutants. It should be noted that both air mass trajectory and CWT analysis are methods to reveal potential sources regions. Compared to the air mass trajectory analysis, CWT has an additional advantage of presenting the spatial distribution of potential sources regions. In this study, we combined air mass trajectory and CWT to identify the source regions of specific air pollutants.

In the CWT method, each grid cell is assigned a weighted concentration by averaging the sample concentrations that have associated trajectories crossing the grid cell as follows:

$$C_{ij} = \frac{1}{\sum_{l=1}^{M} \tau_{ijl}} \sum_{l=1}^{M} C_l \tau_{ijl} \quad (1)$$

where C_{ij} is the average weighted concentration in the ijth cell, l is the index of the trajectory, M is the total number of trajectories, C_l is the concentration observed on the arrival of trajectory l, and τ_{ijl} is the time spent in the ijth cell by trajectory l. A high value for C_{ij} is implies that air parcels traveling over the ijth cell would be, on average, associated with high concentrations at the receptor.

To eliminate the uncertainty of C_{ij} is caused by low n_{ij} values, every C_{ij} is should be multiplied by an arbitrary weight function W_{ij} to get more accurate results. The weight function W_{ij} to is defined as:

$$W(n_{ij}) = \begin{cases} 1.0 & 3n_{ave} < n_{ij} \\ 0.7 & 1.5n_{ave} < n_{ij} \le 3n_{ave} \\ 0.4 & n_{ave} < n_{ij} \le 1.5n_{ave} \\ 0.2 & n_{ij} \le n_{ave} \end{cases}$$

n_{ave} represents the average number of trajectories in grid cells with trajectories passing through the partition region; n_{ij} is the number of all trajectories in the (i, j) cell.

2.3.3. EC-tracer method

Organic carbon (OC) and elemental carbon (EC) were the major components of fine particles ($PM_{2.5}$) (Malm et al., 2004). EC was a product of the carbon-based fuel combustion process and was considered entirely derived from primary emissions, while OC can be derived from both primary emissions and second formation. SOC (secondary organic carbon) can be estimated using EC as a tracer as below (Turpin and Huntzicker, 1994),

$$POC=(OC/EC)_{pri}\times EC \quad (2)$$

$$SOC=OC-(OC/EC)_{pri}\times EC \quad (3)$$

Where $(OC/EC)_{pri}$ is the OC/EC ratio of freshly combusted aerosols. To determine the values of $(OC/EC)_{pri}$, it is firstly assumed that the $(OC/EC)_{pri}$ values varied continuously. Then we calculated the corresponding SOC concentrations based on each hypothesized $(OC/EC)_{pri}$ value and the correlation coefficient (R^2) of the SOC and EC pair (i.e., R^2 (EC, SOC)). Thus, a series of R^2 (EC, SOC) values can be plotted against the OC/EC ratios. Since the sources of EC and SOC were independent, the OC/EC ratio corresponding to the minimum R^2 (EC, SOC) was considered to be $(OC/EC)_{pri}$ (Wu and Yu, 2016).

3 Results and Discussion

3.1 Air quality and weather conditions during the whole study period

The whole study period was divided into five stages: S1 (15-23 August), S2 (24-27 August), S3 (28 August-3 September), S4 (4-6 September), and S5 (7-12 September). S1 was the reference stage without intense emissions control measures. S2 was the stage of industrial and construction emissions control. In detail, the emission control on industries was implemented during 24-25 August. Enterprises in Hangzhou were either temporally suspended or reducing productions. After 25 August, construction activities were prohibited. S3 added restriction on the motor vehicles. The odd-even traffic rule was fully implemented and vehicles from outside Hangzhou were prohibited from entering the city. In addition, transportation of dusty materials was not allowed during this period. S4 was the G20 Summit period, which was the most stringent emission control stage with the implementation of emergency controls on VOC and $PM_{2.5}$ precursors emissions based on the air quality forecasting if a pollution day was predicted. S5 was the post-G20 stage with all the control measures lifted.

The time series of hourly $PM_{2.5}$, PM_{10}, and its precursors (SO_2, NOx) are illustrated in Fig. 2, together with the meteorological parameters (i.e., wind speed (WS), wind direction (WD), temperature (T), relative humidity (RH), radiation, and boundary layer height (BLH)). As shown in Fig. 2, the easterlies dominated during S1, S4, and S5. The winds changed from easterlies to westerlies in S2 and turned to be from the southwest in S3. The average wind speed from S1 to S5 was 1.34, 1.68, 1.30, 1.31, and 0.96 m s^{-1}, respectively. RH in S3 was obviously lower than the other stages while it reached high in S5. Temperature were the highest in S1 and S2 then gradually decreased in S3, finally declining quickly in S4 and S5. Radiation was high during the first three stages (mean value of 301, 357, and 433W m^{-2}), especially in S3. It turned to be weaker during the last two stages (mean value of 204 and 215 W m^{-2}). The variation of boundary layer height was as similar as radiation to some extent. It was high from S1 to S3 but quickly became shallow in S4 and S5. S2 was the stage of industries and construction emission control accompanied with the highest wind speed, the concentrations of NOx, SO_2, and PM all dropped to low levels. It should be noted that although S3 added the emission control measures on motor vehicles, the concentrations of NOx remained at relatively high levels even under favorable meteorological conditions such as high wind speed, strong radiation, and low relative

humidity. This phenomenon will be discussed later. Since S4 was the most stringent emission control period, all the air pollutants were greatly reduced although the meteorological conditions were unfavorable due to relatively low wind speed and high RH. However, a short pollution episode occurred on the morning of September 4 with the hourly $PM_{2.5}$ concentration exceeding 100 μg m^{-3}. After all the control measures were lifted in S5, $PM_{2.5}$ rebounded associated with unfavorable weather conditions (i.e. low wind speed and BLH, weak radiation, and high RH). The average concentrations of $PM_{2.5}$ during the five stages were 37.4, 31.8, 40.4, 35.0, and 49.5 μg m^{-3}, respectively. On the whole, the $PM_{2.5}$ concentrations during control stages were lower than the reference and post-G20 stages.

3.2 Diurnal profiles of $PM_{2.5}$ species and meteorological variables

The diurnal variations of $PM_{2.5}$ major compositions, as well as the key meteorological parameters, were demonstrated in Fig. 3 for all the five stages. As for the meteorological parameters, in general, RH, T, and WS exhibited consistent diurnal trends among the five stages. RH was relatively low during daytime and high during nighttime while temperature showed the opposite trend. Wind speed was relatively low during the first half of the day and gradually increased in the afternoon.

During all the stages, NOx exhibited peak values at around 6:00~8:00 AM LT (Local Time) and 16:00~20:00 PM LT, corresponding to the morning and evening rush hours due to the enhanced vehicular emissions. In S4 which was the G20 period, the evening peak of NO_X was almost missing and this should be attributed to the stringent emission control during that period. While in S5, in addition to the peaks during the morning and evening rush hours, NO_X showed significant enhancement around the daybreak from around 21:00 PM to 3:00 AM LT. This was ascribed to the allowance of heavy-duty diesel trucks into Hangzhou during night-time after G20. This phenomenon was also reflected by the corresponding EC and OC peaks around the similar period. In contrast, the high concentrations of SO_2 and SO_4^{2-} mainly appeared from 6:00 AM to 18:00 PM LT, tracking well with the working hours. Power plants and industries were the major contributors to SO_2 emissions and they were mainly operating during daytime. An exception was noted that the diurnal variation of sulfate in S5 was different from the other four stages, and its peak appeared in the early morning and night. The low sulfate levels during daytime were likely due to the low secondary conversion rate associated with weak radiation and low temperature in this stage. In addition, there were sustained precipitation

events during daytime on September 7th and September 9th (Fig. S1), which could have reduced the sulfate concentrations during daytime to some extent. The high levels of sulfate during daybreak and night may be related to the heterogeneous reaction due to the high RH and PM. High PM concentrations in S5 provided enough surface area for the conversion of sulfate under high RH conditions (Mattias Hallquist, 2016).

POC and SOC were differentiated in five stages based on the method described in Sect. 2.2.3. As shown in Fig. 3, POC in all five stages maintained at certain levels without dramatic diurnal fluctuations. In contrast, SOC in S1, S2, and S5 showed a tendency to increase starting from the early morning and reached a maximum in the midday, indicating the photochemical formation of SOC. This is consistent with previous studies that photochemical pathways were of importance for the formation of SOC (Wyche et al., 2014;Liu et al., 2015b;Kleeman et al., 2007;Xu et al., 2017). Unlike the three stages above, there were noticeable absences of SOC peaks around the midday in S3 and S4, resulting in ambiguous diurnal fluctuations. The stringent emission control measures should exert a significant impact on the SOC formation due to the great reduction of its precursors. Furthermore, the concentrations of SOC showed a positive relationship with temperature (Fig. S2). Under relatively low temperature, the concentrations of SOC stayed at relatively low levels and increased greatly with the increase of temperature, indicating an enhanced role of higher temperature in SOC formation in summer. In this regard, the relatively low temperature in S3 and S4 may also explain the low SOC concentrations during these two stages. Although S2 was also the emission control stage, no absence of SOC peaks during daytime was observed as shown in Fig. 3. On the one hand, S2 was the weakest emission control stage without adding the emission control on vehicles, which were important sources of VOCs. Therefore, the impact of emission control measures on SOC formation at this stage was not as significant as S3 and S4. On the other hand, the relatively high temperature and strong radiation intensity in S2 may be favorable for the SOC formation. As for the relationship between SOC and RH, no clear correlation was observed in this study, which was as similar as that observed in Beijing (Zheng et al., 2015). Overall, we found that the emission controls had an evident suppressing impact on the SOC formation and crucial meteorological parameters (e.g. temperature and radiation) were also of importance.

3.3 Aerosol chemical composition

Fig. 4a shows the comparison of aerosol chemical components among the five stages. The major components of $PM_{2.5}$ were identified as SNA (SO_4^{2-}, NO_3^-, and NH_4^+), EC, and OM, which together

accounted for approximate 60-80 % of the aerosol masses during different stages (Fig. 4b). The sum of SNA, EC, and OM decreased with different extents from S2 to S4 compared to S1, demonstrating the effectiveness of emission control measures in Hangzhou and its surroundings on the improvement of air quality. Of which, the decrease of OM was mostly responsible with a reduction percentage of 32 %, 15 %, and 38 % from S2 to S4 compared to S1. The reductions of EC were 21 %, 18 %, and 23 % from S2 to S4 compared to S1. This suggested that the emission control measures played a significant role in reducing the carbonaceous aerosols. On the opposite, SNA increased 8 % and 43 % in S3 and S4, respectively. This highlighted SNA was more enhanced during the emission control stages under variable meteorological conditions. Specifically, the average concentrations of SO_4^{2-} in S3 (5.4 μg m^{-3}) and NO_3^- in S4 (3.9 μg m^{-3}) were higher than those of S1 (SO_4^{2-}:4.4 μg m^{-3}; NO_3^-: 2.2 μg m^{-3}). Given that both S3 and S4 were the intense emission control periods, the unexpected increases of secondary aerosol components may be attributed to the long-range transport or unfavorable meteorological conditions. More detailed analysis will be presented in Sect. 3.4. After the G20 Summit, the sum of SNA, OM, and EC increased 42 %, 52 %, and 62 % compared to S2-S4, respectively, clearly demonstrating the negative effect of lifting the emissions control measures on deteriorating the air quality.

Fig. 4a. further shows the mass ratios of NO_X/SO_2, NO_3^-/EC, and SO_4^{2-}/EC at each stage. The ratio of NO_X/SO_2 gradually decreased from S1 to S4 as the emission control measures were more intensified, indicating that NO_X emissions were more effectively abated relative to SO_2 emissions. The NO_X/SO_2 ratio rose to the highest in S5, owing to the lifting of emission control measures especially from the traffic sector. The ratios of NO_3^-/EC and SO_4^{2-}/EC can be used to pinpoint the extent of secondary formation by minimizing the effect of different meteorological conditions on the absolute concentrations of aerosol components (Zheng et al., 2015). In other words, the ratios of NO_3^-/EC and SO_4^{2-}/EC can represent the extent of the secondary reactions. As shown in Fig. 4a, the SO_4^{2-}/EC ratios gradually increased during the first three stages, followed by a slight decrease during S4 and S5. Generally, SO_4^{2-}/EC ratios varied within a narrow range of around 3-4, indicating the relatively stable reactions of SO_2 to SO_4^{2-} in the five stages. The variation of NO_3^-/EC showed a different pattern that it remained consistently low during the first three stages and then showed a substantial increase during S4 and S5. NO_3^-/EC ratios in S4 and S5 increased about 2-3 times than those from S1-S3. Moreover, the NO_3^-/EC ratios were lower than SO_4^{2-}/EC during the first four stages while it exceeded SO_4^{2-}/EC in S5.

3.4 Process analysis in each stage

3.4.1. High aerosol species in S1

Fig. 5 shows the time-series of the major aerosol chemical components during the whole study period. In S1, most of the aerosol components maintained at high levels, especially for sulfate, EC, and OC. Since the weather conditions were characterized of the well-developed boundary layer, high temperature, low RH, and moderate WS (Fig. 2), air pollutants were supposed to be subject to efficient diffusion. However, relatively high concentrations of EC and OC, accompanied by the high concentration of NO_X were observed, indicating strong emissions from the traffic sector in S1. In addition, concentrations of sulfate were also at high levels, suggesting the considerable impact from the power grid.

3.4.2. Substantial decreases of aerosol species in S2

S2 was the stage that implemented the industrial and construction emission control measures. Concentrations of SNA, EC and POC were significantly reduced, indicating the great benefits from the emission control strategy.

3.4.3. Influence from long-range transport in S3

A continuously increasing trend of particulate mass concentrations was observed in S3 (Fig. 2), including SO_4^{2-}, NH_4^+, EC, and POC (Fig. 5). The meteorological conditions in this stage were generally favorable for the diffusion of air pollutants as indicated by the low RH, strong radiation, and high BLH (Sect. 3.1). It could be visualized that the high pollution episodes tended to accompany high wind speed (Fig. S3), suggesting the increases of aerosol components may be attributable to the regional or long-range transport. The 72-h backward trajectory clustering analysis was performed during S3 (Fig. 6a). It is shown that most of the backward trajectories were related to the regional/long-range transport with a contribution of more than 60 %, while the rest of the backward trajectories were restrained within the local range. To further identify the potential source regions of specific air pollutants, we conducted the concentration weighted trajectory (CWT) analysis (Fig. 6b-6e).

The results showed fairly consistent CWT spatial patterns for NO_X and NO_3^-, i.e. high NO_X and NO_3^- hotspots were mainly derived from Hebei province, Shandong province, and the conjunction area of Anhui and Jiangsu provinces. This could partly explain why the concentrations of NO_X increased significantly in S3, which was the stage that the motor vehicle emission control measures were fully implemented in Hangzhou. Compared to NO_X and NO_3^-, the potential source regions of SO_2 and SO_4^- exhibited inconsistent spatial patterns. As shown in Fig. 6d-6e, the SO_2 CWT plot indicated hotspots mainly from southern Hebei, Shandong, and Jiangsu provinces, while the potential sources of sulfate were mainly ascribed to regions south of Hangzhou, i.e., the conjunction areas of Jiangxi, Anhui, and Zhejiang provinces. This should be attributed to the impact of meteorological conditions on the formation of sulfate. Table S1 shows the temperature in different areas that the hotspots had covered during the three days before S3 according to the 72h air mass back trajectory in CWT analysis. It is obviously shown that the temperature in the northern regions were much lower than in the southern regions. The high temperature in the south should be favorable for the photochemical formation of sulfate in summer. This could be the reason of the different potential source regions of SO_2 and sulfate.

3.4.4. Impact from continental outflow in S4

S4 was the G20 Summit period, which was the most rigorous emission control stage. However, a high particulate pollution episode occurred with the hourly $PM_{2.5}$ peak concentration of exceeding 100 μg m^{-3} between 0:00-5:00 LT in the morning of 4 September, which was the first day of the G20 Summit. Consistently, concentrations of the major aerosol components also increased substantially (Fig. 7a). If this short pollution episode was absent, the average concentrations of $PM_{2.5}$, SNA, and OC during S4 could be lowered by 12 %, 12 %, and 3 %, respectively. Fig. 7c shows the 48-h air mass backward trajectories during this pollution period and six backward trajectories were computed at 500 AGL from 22:00 LT on 3 September to 8:00 LT on 4 September (22:00, 0:00, 2:00, 4:00, 6:00, 8:00). It is shown that the prevailing air masses were mainly from Hebei, Shandong and then passed over the East China Sea before reaching Hangzhou. As shown in Fig.7a, Cl^- had a dramatic increase from almost zero before 4 September to a peak value of 0.24 μg m^{-3} in the morning of 4 September along with the increase of RH, which further indicated the long-range transport route over the ocean. This implied that the meteorological conditions should be favorable for the heterogeneous reaction pathway of secondary

aerosol formation facilitated by the humid oceanic air masses. As for the potential source regions in Shandong, Fig. S4 plots the concentrations of NO_2 and SO_2 in different urban areas of Shandong province where the trajectories had passed through during the same period. The concentrations of NO_X and SO_2 in Shandong province ranged from 31 to 78 μg m^{-3} and 13 to 56 μg m^{-3}, respectively. The mean values of NO_X and SO_2 were 56 μg m^{-3} and 32 μg m^{-3}, much higher than those of 14 μg m^{-3} and 8 μg m^{-3} in Hangzhou. Hence, the air masses originating from Shandong province should be contributable to the observed high values of aerosol secondary components in the morning of 4 September. However, it is difficult to determine that whether the high concentrations of SNA were dominated by local atmospheric processing or directly transported from the upstream areas. Here, we calculated the time-series of sulfur oxidation ratio (SOR) and nitrogen oxidation ratio (NOR) as shown in Fig. 7b. The NOR and SOR in this study are calculated as molar fraction by the following equations:

$$SOR=\frac{nSO_4^{2-}}{(nSO_4^{2-}+nSO_2)} \quad (4)$$

$$NOR=\frac{nNO_3^-}{(nNO_3^-+nNO_2)} \quad (5)$$

Both SOR and NOR had obvious increases in the morning of 4 September. Of which NOR increased dramatically from a mean value of 0.06 from 0:00 LT on 1 August to 23:00 LT on 3 September to a peak value of 0.52 on 04:00AM LT on 4 September. We do not think a 9-fold increase of NOR within 5 hours was due to the local atmospheric processing. Instead, the massive input of the secondary aerosols via long-range transport should be the major cause of the abrupt increase of SOR and NOR. It has been recognized that secondary formation from the oxidation of NO_X and SO_2 can occur in air masses during the transport and directly resulted in rapid increase of $PM_{2.5}$ (Li et al., 2015). After this short particulate pollution episode, the concentrations of SNA, OC, and EC decreased quickly in the afternoon of September 4, demonstrating the effectiveness of emission control measures during the G20 Summit period. In addition, all those pollutants remained at low levels throughout S4, further manifesting the positive impact on PM reduction caused by emission control strategies.

3.4.5. Rebounce of air pollutants in S5

After the lifting of emission control measures, the concentrations of all the air pollutants quickly climbed, demonstrating an abrupt worsening of air quality after the G20 Summit (Fig. 5). Mean

concentrations of SNA, OC, and EC increased significantly compared to the control stages. In detail, SNA increased 62 %, 52 %, and 37 % compared to S2-S4, respectively, with an average rise of 50 %. OC increased 45 %, 30 %, and 50 % compared to the three stages above, with an average rise of 42 %. As for EC, the increments reached 40 %, 18 %, and 29 % with the mean value of 29 %. The substantial increases of all the air pollutants in the post-control period further corroborated the prominent effect of emission controls on PM reduction during the control period. As described in Sect. 3.1, the meteorological conditions in this stage were characterized of high RH at 46-94 %, low wind speed at 0.05-2.5 m s^{-1} and low radiation at 3-672 W m^{-2}. This suggested that the unfavorable meteorological conditions during S5 should additionally contribute to the deterioration of air quality. Actually, the high concentrations of SNA, OC, and EC were mostly observed at nighttime, accompanied with high RH and low wind speed, elucidating the important role of meteorological conditions in the rise of particulate matters in S5. 72-hours air mass backward trajectory clustering results illustrated that about 20% of the trajectories travelled relatively short distances, which were restrained within the Yangtze River Delta, while the rest of the trajectories were derived from much farther regions (Fig. 8a). This indicated that external transport should contribute almost 80% of the S5 periods from the perspective of synoptic meteorology. However, the CWT results (Fig. 8b-8e) showed that the major potential sources of sulfate and nitrate with their gaseous precursors were mainly dominated by local and regional emissions with highest hotspots around the Hangzhou Bay region. It should be noted that a large number of the hotspots also appeared over the East China Sea as indicated in Fig. 8b-8e. It could be visualized that the plumes over the ocean were linked back to the hotspots over land, specifically from Jiangsu and Shandong provinces, indicating the continental outflows were influential on the high levels of NO_3^-, SO_4^{2-}, and their precursors during the post-G20 period. In addition, the hotspots over the ocean, especially the coastal regions near Shanghai and Hangzhou, maybe related to the emissions from shipping activities. Our sampling site is located in the northeast of Hangzhou, close to the Ningbo-Zhoushan Port, which ranks as the second largest port and has the largest cargo throughput among China's top ten ports. Previous studies have shown that ship emissions have an important impact on the Yangtze River Delta region and Eastern China (Fan et al., 2016;Liu et al., 2016). (Liu et al., 2016) has even shown shipping emissions could contribute 20 - 30% (2 - 7 μg/m^3) of the total $PM_{2.5}$ within tens of kilometers of coastal and riverside Shanghai during ship-plume-influenced periods in

spring and summer. (Fan et al., 2016) estimated the total emissions of SO_2 and NOx reached 3.8×10^5 and 7.1×10^5 tons/yr of the study area (119°E to 125°E and 27°N to 36°N) in 2010, respectively.

3.5 Formation of secondary aerosols

3.5.1. Secondary inorganic aerosols

The formation pathways of sulfate and nitrate were usually dominated by heterogeneous reactions as indicated by previous studies that both these two species showed a strong dependence on relative humidity (Cheng et al., 2014;Pan et al., 2016). However, this study showed contrasting results to those previous studies. Fig.9a & 9b plot the variations of NOR and SOR as a function of RH colored by temperature. In addition, the relationship between NOR (SOR) and RH was investigated by grouping RH into eight bins with an increment of 10 %. As shown in Fig. 9a, NOR was low and fluctuated within a relatively narrow range under low RH conditions (RH<60 %). It is usually recognized that the conversion efficiency from NO_x to NO_3^- via aqueous pathway was relatively low under low RH conditions. Besides, the low RH hours were generally associated with high temperature as indicated by the colored scatters in Fig. 9a. Nitrate was unstable and easy to decompose under high temperature, thus also resulting in low NOR values. As RH increased (RH>60 %), NOR started to quickly increase with the decrease of temperature. In accordance with previous studies, the variation of NOR as function of RH exhibited an exponential growth, manifesting the heterogeneous formation of nitrate. In comparison, the variation of SOR as a function of RH and temperature was totally different from that of NOR (Fig. 9b). The values of SOR fluctuated much more significantly than NOR under almost all the RH conditions, showing ambiguous relationship between SOR and RH. This relationship was further evaluated by grouping all the data into daytime and nighttime. In the daytime, SOR showed an increasing trend with the increase of RH under low RH conditions (RH<50 %), while it showed a slightly decreasing trend as RH increased and reached the lowest under RH > 90 %. As discussed above, the low RH periods were mostly associated with high temperature, which often meant strong radiation as shown in Fig. 2. This was beneficial for generating sufficient hydroxyl radicals and promoting the subsequent photochemical reactions of sulfate formation (Canty, 2002;Matthijsen et al., 1998). While under high RH conditions, the temperature was much lower, which was not favorable for

the photochemical formation of sulfate. This suggested the importance of photochemical formation pathway of sulfate during the whole study period in Hangzhou. Different from daytime, SOR showed an increasing trend with RH in nighttime under the full range of RH conditions, indicating the aqueous processing was also crucial for the formation of sulfate.

The mean values of NOR and SOR in each of the five stages were also shown in Fig. 9a & b. Variations of the staged SOR and NOR showed totally different patterns. The mean values of NOR remained low in the first three stages. However, it increased to high levels in S4 and S5 due to the changed meteorological conditions and the influence of regional/long-range transport. Variation of NOR among the five stages showed a wide range of 0.05-0.15 with a gap of 0.1. In contrast, the SOR values among the five stages varied weakly from 0.22-0.29, suggesting nitrate was more influenced by emissions and the extent of long-range transport than sulfate.

Fig. 9c further shows the relationship between sulfate and nitrate as a function of RH. It is clearly shown that high RH episodes tended to accompany with high nitrate concentrations, whereas a number of high sulfate values appeared during low RH periods. This is quite different from the results observed during the severe haze episodes in Beijing that high levels of both nitrate and sulfate occurred under high RH conditions (Sun et al., 2013;Wang et al., 2016). In Fig. 9d, we also investigated the behavior of SO_2 and NO_X, the precursors of sulfate and nitrate under the computed RH bins. It is found that SO_2 concentrations showed a substantial decrease, while NO_X concentrations increased with increasing relative humidity, suggesting the emissions of sulfate and nitrate precursors also have a great impact on the secondary aerosols formation in addition to the meteorological conditions. Due to the relatively low concentrations of SO_2 under high RH conditions as well as the moderate level of SOR, the low sulfate concentrations were expected as discussed above.

Fig. 9e shows the mass fraction of SNA in $PM_{2.5}$ as a function of RH colored by temperature. The sizes of the circles corresponded to the mass concentrations of $PM_{2.5}$. Generally, the ratios of $SNA/PM_{2.5}$ increased with the elevated RH, demonstrating the significant enhancement of SNA formation under high RH conditions. An exception should be noted that in the RH bin of 90-100 %, the $SNA/PM_{2.5}$ ratio increased to an abnormally high value of 0.65. All data in this RH bin comes from 7 September, which was a rainy day with accumulated precipitation of 9.5 mm (Fig. S1). Accordingly, the $PM_{2.5}$ concentrations averaged within this RH bin were the lowest according to the size of the circles as shown in Fig. 9e. Thus, this data point was excluded in the following discussion. Compared

to the study in Beijing (Wu et al., 2018) which showed more obvious increase of the SNA/$PM_{2.5}$ ratio from 24 % to 55 % during the average RH from 15 % to 83 %, this study showed weaker increase of the SNA/$PM_{2.5}$ ratio from 23 % to 43 % in the similar RH range. This could be partly attributed to that the formation of sulfate was not very sensitive to RH as shown in Fig. 9b. In addition, our results showed that the mass concentrations of $PM_{2.5}$ didn't present an increasing trend as RH increased, which was different from (Wu et al., 2018). In detail, (Wu et al., 2018) found significant increases of $PM_{2.5}$ concentrations from an average of 39.4 μg m^{-3} under RH < 20 % to 98.7 μg m^{-3} under RH within 60-70 %, suggesting a feedback mechanism between the aerosol liquid water and uptake of inorganic matters. Fig. 9e shows the highest $PM_{2.5}$ concentrations occurred under the medium levels of RH, e.g. 40-60 % but not necessary under high RH conditions. It should be noted that the average $PM_{2.5}$ concentration in this study was 39.3 μg m^{-3}, much lower than that of Beijing due to less strong emission intensities. In this regard, the level of $PM_{2.5}$ over the study region should be vulnerable to the inputs of outside air pollutants, especially during the emission control period.

We further investigated the average SNA/$PM_{2.5}$ ratios and $PM_{2.5}$ concentrations during the five stages as marked by the open circles in Fig. 9e. The SNA/$PM_{2.5}$ ratios of S4 and S5 largely deviated from the statistical curve between SNA/$PM_{2.5}$ and RH. As discussed in Section 3.4, regional and long-range transport were ubiquitous during S4 and S5. Thus, it was likely that the input of transported air pollutants disturbed the relationship between $PM_{2.5}$ and RH to some extent. As for S3, although transport evidence was also revealed during this stage, the extent of long-range transport was relatively weak, which will be discussed in Section 3.6. Hence, the mean SNA/$PM_{2.5}$ ratio and $PM_{2.5}$ concentration during S3 still coincided with the statistical curve. Overall, the relationship between $PM_{2.5}$ concentrations and RH was ambiguous, which was attributed to the net effects of regional/long-range transport and emission control.

3.5.2. Secondary organic aerosols

The average OC/EC ratios were 4.0, 3.6, 4.2, 4.2, and 4.5 during the five stages with the average value of 4.1. It has been recognized that if OC/EC ratios exceeding 2.0, there is production of secondary organic aerosol (Cao et al., 2013). Hence, the mean ratio of OC/EC in this study implied the substantial

formation of SOC during the whole study, which was ascribed to the humid and warm weather conditions in the summer and autumn of Hangzhou.

As introduced in Sect. 2.3.3, the EC-tracer method derived the $(OC/EC)_{pri}$ values in the range of 1.7 to 2.9 (Fig. S5), which were within or slightly higher than the $(OC/EC)_{pri}$ values of (1.15-1.85) derived by (Wu et al., 2016). Due to the implementation of different control strategies, the $(OC/EC)_{pri}$ values fluctuated greatly among the five stages as shown in Table 1.

The average SOC concentrations were estimated to be 3.8, 2.2, 2.0, 1.8, and 2.2 μg m^{-3} from S1 to S5, respectively. The highest SOC concentration along with the highest SOC/OC ratio (0.5) in S1 can be partly explained by the possibly high abundance of SOC precursors before implementation of the intense emission control measures. In addition, the highest temperature and solar radiation in S1 should be also responsible for the strong formation of SOC (Fig. S2 in Sect. 3.2). During S2-S4, the concentrations of SOC evidently decreased compared to S1 while those of POC stayed at similar levels as S1, thus resulting in an obvious decrease of the SOC/OC ratios. This should be mainly ascribed to the abatement of SOC precursors, e.g. VOCs. The restrictions on vehicle stocks, construction works, and giving local residents extra holiday should greatly reduce the VOC emissions from vehicles, painting, residential and restaurant cooking, etc. The lowest concentrations of SOC during the intense control stages reflected the effectiveness of the emission control measures on suppressing the formation of secondary organic aerosols. During S5, SOC had a slight rebounce compared to the control stages while POC increased substantially to an average of 6.2 μg m^{-3}, about 50-150 % higher than the previous stages. As a result, the extremely low SOC/OC (0.22), namely the very high POC/OC ratio (0.78) was estimated. This suggested the primary carbonaceous emissions were greatly enhanced after the lifting of various emission control measures. Allowance of all types of vehicles after the G20 Summit should be the major factor contributing to the elevated primary carbonaceous aerosols. In addition, recovery of industries and construction works should be also partly responsible for this.

Table S2 summarizes the SOC/OC ratios in different urban areas. Generally, the average SOC/OC ratios in this study were lower than previous studies. Compared to the previous studies in Hangzhou, (Li et al., 2017a) estimated a SOC/OC ratio of around 40 %, slightly higher than this study. However, the study by (Li et al., 2017a) was conducted in winter, thus the SOC/OC ratio should be considered as a lower limit. Compared to the results in (Jiao and Qi, 2007), the SOC/OC ratio in summer was 45.8 %,

much higher than this study. All the results above indicated the intense emission control measures had exerted significantly negative impacts on the formation of secondary organic aerosols.

3.6 Diagnose the effect of regional/long-range transport

Fig. 10 shows the relationship between hourly sulfate/nitrate and EC during different time periods. Three periods were defined, of which Fig. 10a & 10b consisted of all the data by excluding the regional and long-range transport episodes as identified in the earlier discussions. It was obviously shown that sulfate/nitrate and EC were weakly correlated. This is expected as EC is a primary particulate pollutant emitted from incomplete combustion while sulfate and nitrate are formed from secondary reactions. As a comparison, sulfate and EC exhibited a moderate correlation (r^2 = 0.40) during S3 (Fig. 10c), which was a period identified with intensive long-range transport (Sect. 3.4.3). This phenomenon was more evident in the quick pollution episode in S4 (Fig. 10d). Sulfate showed significant correlation with EC (r^2 = 0.67) and a moderate correlation was also observed between nitrate and EC (r^2 = 0.40). This "abnormally" positive correlation between species that were derived from different sources and formation pathways indicated that the temporal variations of aerosol components were dominated by physical processes rather than atmospheric chemical processing. That is to say, it was driven by the transport which brought massive inputs of air pollutants, and then diluted or accumulated synchronously. Hence, to assess whether there is a significant correlation between EC and secondary aerosol components could possibly judge the occurrence and extent of regional and long-range transport.

Fig. 11 further evaluated the effect of regional/long-range transport on the extent of the formation of secondary inorganic aerosols (i.e. the SNA/EC ratio) and $PM_{2.5}$ levels by grouping each stage to a wind direction bin of 45 degrees. All data were colored by wind speed and the sizes of the filled circles corresponded to the $PM_{2.5}$ concentrations. It is clearly shown that in S1 both the SNA/EC ratios and $PM_{2.5}$ concentrations became relatively high from the northeast and northwest, i.e. the upstream polluted regions with much higher emission intensities than the Yangtze River Delta. Statistically, the SNA/EC ratios from the wind sectors of northwest to northeast were moderately higher (1.4-fold) than from the other directions, suggesting the regional transport was not prominent. S2 generally exhibited a similar pattern as S1. The difference was the overall decrease of $PM_{2.5}$ concentrations from all the wind

583 sectors. This was partly ascribed to the emission control and was also related to the higher wind speed
584 as visualized by the colored circles.
585 Compared to S1and S2, S3 showed an opposite pattern of SNA/EC as a function of wind direction.
586 The relatively high SNA/EC ratios were observed anti-clockwise from the northeast to southwest as
587 well as for the $PM_{2.5}$ concentrations as well as for the $PM_{2.5}$ concentrations. This was consistent with
588 the CWT results that the southern areas of Hangzhou were the potential source regions of high sulfate
589 and nitrate (Sect. 3.4.3). It should be noted that although regional transport was observed during this
590 stage, the SNA/EC ratios from the northeast to southwest were only 18-27 % higher than the other
591 directions, much lower than the regional transport from the north as discussed below. We think this was
592 due to that the southern part of the Yangtze River Delta had lower emission intensities than the north,
593 thus limiting the elevation of the SNA/EC ratios during the transport.
594 In S4, a distinctly different pattern of SNA/EC from the other stages showed the extremely high
595 ratios of SNA/EC from the north and northeast, about 2.4-3.4 times that from the other directions. This
596 corroborated with the air mass backward trajectory analysis in Fig. 7, verifying the transport path in the
597 form of continental outflows. The high ratios of SNA/EC from the north and northeast in S4 were
598 almost 4 times higher than the other four stages, which was also consistent with the discussions in
599 Section 3.4.4 that SOR and NOR abruptly increased during the quick pollution episode in the morning
600 of 4 September. Specifically, the two highest SNA/EC ratios were accompanied with large error bars,
601 suggesting the great fluctuations of SNA/EC in the divided wind direction intervals. This was related to
602 the characteristics of the oceanic air masses from the north to the east. In most circumstances, the
603 oceanic air masses directly from the ocean exerted cleansing effect, lowering the levels of air pollutants.
604 However, the oceanic air masses originating from land in S4 could have transported abundant air
605 pollutants back to the downstream areas, worsening the air quality in this study. Thus, the $PM_{2.5}$ levels
606 associated with the oceanic air masses could have been in a wide range, thus generating large SNA/EC
607 error bars.
608 As for S5, the pattern of SNA/EC as a function of wind direction was somewhat as similar as S1 and
609 S2. The values of SNA/EC were much higher than those of S1-S3 in almost all the wind direction
610 intervals. Lifting of emission control measures should be the major cause. In addition, unfavorable
611 meteorological conditions (e.g. low wind speed for the high SNA/EC groups) also accelerated the
612 formation and accumulation of secondary aerosols.

4 Conclusions

In this study, atmospheric chemical compositions from 15 August to 12 September before, during, and after the 2016 Hangzhou G20 Summit were monitored. Water-soluble ions, organic/elemental carbon, and gaseous pollutants were continuously measured. Soluble ions and carbonaceous matters were the major components of fine particles, accounting for 60-80 % of $PM_{2.5}$. The average $PM_{2.5}$ concentrations during the five defined stages (one reference stage, three control stages, and one post-G20 stage) were 37.4, 31.8, 40.4, 35.0, and 49.5 μg m^{-3}, respectively. In general, the emission control measures were effective in lowering the concentrations of fine particles. The impact of emission control measures on perturbing the air quality was fully assessed. The major findings are summarized as below.

1. Both sulfate and nitrate showed dependence on RH, but RH played a more important role in the formation of nitrate. In addition, the formation of sulfate was found highly related to the photochemical reactions, especially during daytime. This is different from previous studies on haze in Beijing that the formation of sulfate was more influenced by RH.
2. Air mass backward trajectory and CWT analysis suggested that regional/long-range transport were ubiquitous even during the strict vehicle stock control period. Long-range transport from upstream regions such as Shandong and Jiangsu was diagnosed as the main cause of high NOx concentrations.
3. One high particulate pollution episode observed in the morning of 4 September (the first day of the G20 Summit) was found related to the continental outflow travelling over the East China Sea. Abrupt increases of SOR and NOR values were observed during this short pollution episode, especially for NOR with a 9-fold increase within 5 hours. Local atmospheric processing in Hangzhou shouldn't be the driving force. Instead, the formation of secondary aerosols in the humid oceanic air masses or direct inputs of secondary aerosols from upstream source regions were responsible for this most severe particulate pollution during the study period.
4. The concentrations of estimated SOC showed significant decreases during all the control stages. Specifically, the SOC diurnal pattern was modified and its peaks in the daytime were greatly reduced, indicating the influence of emission control effects on the SOC formation.

This study shows that the various emissions control measures implemented during the Hangzhou G20 Summit indeed had a positive impact on the reductions of aerosol concentrations in a short period of

time. However, the regional/long-range transport may offset the local emission control effects to some extent. Finally, the post-G20 period showed a quick and sustained deterioration of air quality, which was as similar as the 2010 Shanghai Expo and 2014 Beijing APEC when all the emission control measures were lifted.

Acknowledgments

This work was financially supported by the National Key Research and Development Program of China (2018YFC0213100), National Natural Science Foundation of China (91644105, 41429501) and Hangzhou Science and Technology Development Plan (20160533B83, 20172016A07).

Data availability. All data used in this paper are available by contacting Kan Huang (huangkan@fudan.edu.cn).

Competing interests. The authors declare that they have no conflict of interest.

References

Canty, T.: Seasonal and solar cycle variability of OH in the middle atmosphere, JGR, 107, 10.1029/2002jd002278, 2002.

Cao, J. J., Zhu, C. S., Tie, X. X., Geng, F. H., Xu, H. M., Ho, S. S. H., Wang, G. H., Han, Y. M., and Ho, K. F.: Characteristics and sources of carbonaceous aerosols from Shanghai, China, Atmospheric Chemistry and Physics, 13, 803-817, 10.5194/acp-13-803-2013, 2013.

Chen, C., Sun, Y. L., Xu, W. Q., Du, W., Zhou, L. B., Han, T. T., Wang, Q. Q., Fu, P. Q., Wang, Z. F., Gao, Z. Q., Zhang, Q., and Worsnop, D. R.: Characteristics and sources of submicron aerosols above the urban canopy (260 m) in Beijing, China, during the 2014 APEC summit, Atmospheric Chemistry and Physics, 10.5194/acp-15-12879-2015, 2015.

Cheng, Y., He, K. B., Du, Z. Y., Zheng, M., Duan, F. K., and Ma, Y. L.: Humidity plays an important role in the PM(2).(5) pollution in Beijing, Environ. Pollut., 197, 68-75, 10.1016/j.envpol.2014.11.028, 2014.

Cheng, Y., Zheng, G., Wei, C., Mu, Q., Zheng, B., Wang, Z., Gao, M., Zhang, Q., He, K., Carmichael, G., Pöschl, U., and Su, H.: Reactive nitrogen chemistry in aerosol water as a source of sulfate during haze events in China, Science Advance, 2016.

Draxler, R., and Rolph, G.: HYSPLIT - Hybrid Single Particle Lagrangian Integrated Trajectory Model, 2012.

Fan, Q., Zhang, Y., Ma, W., Ma, H., Feng, J., Yu, Q., Yang, X., Ng, S. K., Fu, Q., and Chen, L.: Spatial and Seasonal Dynamics of Ship Emissions over the Yangtze River Delta and East China Sea and Their Potential Environmental Influence, Environ. Sci. Technol., 50, 1322-1329, 10.1021/acs.est.5b03965, 2016.

Garrett, T. J., and Zhao, C.: Increased Arctic cloud longwave emissivity associated with pollution from mid-latitudes, Nature, 440, 787-789, 10.1038/nature04636, 2006.

Guo, S., Hu, M., Zamora, M. L., Peng, J., Shang, D., Zheng, J., Du, Z., Wu, Z., Shao, M., Zeng, L., Molina, M. J., and Zhang, R.: Elucidating severe urban haze formation in China, Proc Natl Acad Sci U S A, 111, 17373-17378, 10.1073/pnas.1419604111, 2014.

He, H., Wang, Y., Ma, Q., Ma, J., Chu, B., Ji, D., Tang, G., Liu, C., Zhang, H., and Hao, J.: Mineral dust and NOx promote the conversion of SO2 to sulfate in heavy pollution days, Sci Rep, 4, 4172, 10.1038/srep04172, 2014.

Hsu, Y. K., Holsen, T. M., and Hopke, P. K.: Comparison of hybrid receptor models to locate PCB sources in Chicago, Atmos. Environ., 37, 545-562, 2003.

Huang, K., Zhuang, G., Lin, Y., Fu, J. S., Wang, Q., Liu, T., Zhang, R., Jiang, Y., Deng, C., Fu, Q., Hsu, N. C., and Cao, B.: Typical types and formation mechanisms of haze in an Eastern Asia megacity, Shanghai, Atmospheric Chemistry and Physics, 12, 105-124, 10.5194/acp-12-105-2012, 2012.

Huang, K., Zhang, X., and Lin, Y.: The “APEC Blue” phenomenon: Regional emission control effects observed from space, Atmospheric Research, 10.1016/j.atmosres.2015.04.018, 2015.

Jansen, R. C., Shi, Y., Chen, J., Hu, Y., Xu, C., Hong, S., Li, J., and Zhang, M.: Using hourly measurements to explore the role of secondary inorganic aerosol in $PM_{2.5}$ during haze and fog in Hangzhou, China, AdAtS, 31, 1427-1434, 10.1007/s00376-014-4042-2, 2014.

Jiao, L., and Qi, G.: Characteristics of organic and elemental carbon in PM_{10} over Hangzhou atmosphere, Journal of the Graduate School of the Chinese Academy of Sciences, 24, 625-629, 2007.

Khoder, M. I.: Atmospheric conversion of sulfur dioxide to particulate sulfate and nitrogen dioxide to particulate nitrate and gaseous nitric acid in an urban area, Chemosphere, 49 (2002) 675-684, 2002.

Kim, J. J., Huen, K., Adams, S., Smorodinsky, S., Hoats, A., Malig, B., Lipsett, M., and Ostro, B.: Residential traffic and children's respiratory health, Environ. Health Perspect., 116, 1274-1279, 10.1289/ehp.10735, 2008.

Kleeman, M. J., Ying, Q., Lu, J., Mysliwiec, M. J., Griffin, R. J., Chen, J., and Clegg, S.: Source apportionment of secondary organic aerosol during a severe photochemical smog episode, Atmos. Environ., 41, 576-591, 10.1016/j.atmosenv.2006.08.042, 2007.

Li, L., Dai, Q., Bi, X., Gao, J., Yang, J., Hong, S., and Feng, Y.: Characteristics and sources of carbonaceous species in atmospheric $PM_{2.5}$ during winter in Hangzhou city, Research of Environmental Sciences, 30, 2017a.

Li, P., Yan, R., Yu, S., Wang, S., Liu, W., and Bao, H.: Reinstate regional transport of $PM_{2.5}$ as a major cause of severe haze in Beijing, Proc Natl Acad Sci U S A, 112, E2739-2740, 10.1073/pnas.1502596112, 2015.

Li, P., Wang, L., Guo, P., Yu, S., Mehmood, K., Wang, S., Liu, W., Seinfeld, J. H., Zhang, Y., Wong, D. C., Alapaty, K., Pleim, J., and Mathur, R.: High reduction of ozone and particulate matter during the 2016 G20 summit in Hangzhou by forced emission controls of industry and traffic, Environmental Chemistry Letters, 15, 709-715, 10.1007/s10311-017-0642-2, 2017b.

Li, X., He, K., Li, C., Yang, F., Zhao, Q., Ma, Y., Cheng, Y., Ouyang, W., and Chen, G.: $PM_{2.5}$ mass, chemical composition, and light extinction beforeand during the 2008 Beijing Olympics, Journal Of Geophysical Research: Atmospheres, 118, 12,158–12,167, 10.1002/2013JD020106, 2013.

Liao, H., Chen, W. T., and Seinfeld, J. H.: Role of climate change in global predictions of future tropospheric ozone and aerosols, JGR, 111, 10.1029/2005jd006852, 2006.

Lin, Y., Cheng, M., Ting, W., and Yeh, C.: Characteristics of gaseous HNO_2, HNO_3, NH_3 and particulate ammonium nitrate in an urban city of Central Taiwan, Atmos. Environ., 40, 4725-4733, 10.1016/j.atmosenv.2006.04.037, 2006.

Liu, G., Li, J., Wu, D., and Xu, H.: Chemical composition and source apportionment of the ambient $PM_{2.5}$ in Hangzhou, China, Particuology, 18, 135-143, 10.1016/j.partic.2014.03.011, 2015a.

Liu, H., Liu, C., Xie, Z., Li, Y., Huang, X., Wang, S., Xu, J., and Xie, P.: A paradox for air pollution controlling in China revealed by "APEC Blue" and "Parade Blue", Sci Rep, 6, 34408, 10.1038/srep34408, 2016a.

Liu, T., Wang, X., Deng, W., Hu, Q., Ding, X., Zhang, Y., He, Q., Zhang, Z., Lü, S., Bi, X., Chen, J., and Yu, J.: Secondary organic aerosol formation from photochemical aging of light-duty gasoline vehicle exhausts in a smog chamber, Atmospheric Chemistry and Physics, 15, 9049-9062, 10.5194/acp-15-9049-2015, 2015b.

Liu, Z., Lu, X., Feng, J., Fan, Q., Zhang, Y., and Yang, X.: Influence of Ship Emissions on Urban Air Quality: A Comprehensive Study Using Highly Time-Resolved Online Measurements and Numerical Simulation in Shanghai, Environmental Science & Technology, 51, 202-211, 10.1021/acs.est.6b03834, 2016b.

Malm, W. C., Schichtel, B. A., Pitchford, M. L., Ashbaugh, L. L., and Eldred, R. A.: Spatial and monthly trends in speciated fine particle concentration in the United States, Journal of Geophysical Research: Atmospheres, 109, n/a-n/a, 10.1029/2003jd003739, 2004.

Matthijsen, J., Suhre, K., Rosset, R., Eisele, F. L., Mauldin, R. L., and Tanner, D. J.: Photodissociation and UV radiative transfer in a cloudy atmosphere: Modeling and measurements, Journal of Geophysical Research: Atmospheres, 103, 16665-16676, 10.1029/97jd02989, 1998.

Mattias Hallquist, J. M., Min Hu, Tao Wang: Photochemical smog in China scientific challenges and implications for air-quality policies, National Science Review, 3, 401-403, 2016.

Menon, S., Unger, N., Koch, D., Francis, J., Garrett, T., Sednev, I., Shindell, D., and Streets, D.: Aerosol climate effects and air quality impacts from 1980 to 2030, Environmental Research Letters, 3, 024004, 10.1088/1748-9326/3/2/024004, 2008.

Pan, Y., Wang, Y., Zhang, J., Liu, Z., Wang, L., Tian, S., Tang, G., Gao, W., Ji, D., Song, T., and Wang, Y.: Redefining the importance of nitrate during haze pollution to help optimize an emission control strategy, Atmos. Environ., 10.1016/j.atmosenv.2016.06.035, 2016.

Pathak, R. K., Wu, W. S., and Wang, T.: Summertime PM2.5 ionic species in four major cities of China: nitrate formation in an ammonia-deficient atmosphere, Atmospheric Chemistry and Physics, 2009.

Qiao, Q., Huang, B., Piper, J. D. A., Biggin, A. J., and Zhang, C.: The characteristics of environmental particulate matter in the urban area of Beijing China during the 2008 Olympic Games, Atmospheric Pollution Research, 10.1016/j.apr.2016.08.003, 2016.

Richards, L. W.: Comments on the Oxidation of No2 to Nitrate - Day and Night, Atmos. Environ., 17, 397-402, 1983.

Russell, A. G., Cass, G. R., and Seinfeld, J. H.: On Some Aspects of Nighttime Atmospheric Chemistry, Environmental Science & Technology, 20, 1167-1172, 1986.

Sander, S. P., and Seinfeld, J. H.: Chemical-Kinetics of Homogeneous Atmospheric Oxidation of Sulfur-Dioxide, Environmental Science & Technology, 10, 1114-1123, 1976.

Schleicher, N., Norra, S., Chen, Y., Chai, F., and Wang, S.: Efficiency of mitigation measures to reduce particulate air pollution--a case study during the Olympic Summer Games 2008 in Beijing, China, Sci. Total Environ., 427-428, 146-158, 10.1016/j.scitotenv.2012.04.004, 2012.

Schryer, D. R.: Heterogeneous Atmospheric Chemistry, American Geophysical Union, 1982.

Sun, Y., Wang, Z., Wild, O., Xu, W., Chen, C., Fu, P., Du, W., Zhou, L., Zhang, Q., Han, T., Wang, Q., Pan, X., Zheng, H., Li, J., Guo, X., Liu, J., and Worsnop, D. R.: "APEC Blue": Secondary Aerosol Reductions from Emission Controls in Beijing, Sci Rep, 6, 20668, 10.1038/srep20668, 2016.

Sun, Y. L., Wang, Z. F., Fu, P. Q., Yang, T., Jiang, Q., Dong, H. B., Li, J., and Jia, J. J.: Aerosol composition, sources and processes during wintertime in Beijing, China, Atmospheric Chemistry and Physics, 13,

762 4577-4592, 10.5194/acp-13-4577-2013, 2013.
763 Tie, X., and Cao, J.: Aerosol pollution in China: Present and future impact on environment, Particuology, 7,
764 426-431, 10.1016/j.partic.2009.09.003, 2009.
765 Turpin, B. J., and Huntzicker, J. J.: Identification of secondary organic aerosol episodes and quantitation of
766 primary and secondary organic aerosl cocentration during SCAQS, Atmospheric Chemistry and Physics,
767 1994.
768 Wang, G., Zhang, R., Gomez, M. E., Yang, L., Levy Zamora, M., Hu, M., Lin, Y., Peng, J., Guo, S., Meng, J., Li, J.,
769 Cheng, C., Hu, T., Ren, Y., Wang, Y., Gao, J., Cao, J., An, Z., Zhou, W., Li, G., Wang, J., Tian, P.,
770 Marrero-Ortiz, W., Secrest, J., Du, Z., Zheng, J., Shang, D., Zeng, L., Shao, M., Wang, W., Huang, Y., Wang,
771 Y., Zhu, Y., Li, Y., Hu, J., Pan, B., Cai, L., Cheng, Y., Ji, Y., Zhang, F., Rosenfeld, D., Liss, P. S., Duce, R. A.,
772 Kolb, C. E., and Molina, M. J.: Persistent sulfate formation from London Fog to Chinese haze, Proc Natl
773 Acad Sci U S A, 113, 13630-13635, 10.1073/pnas.1616540113, 2016.
774 Wang, P., and Dai, X.-G.: "APEC Blue" association with emission control and meteorological conditions detected
775 by multi-scale statistics, Atomspheric Research, 178-179, 497-505, 10.1016/j.atmosres.2016.05.001, 2016.
776 Wang, Q., Zhuang, G., Huang, K., Liu, T., Deng, C., Xu, J., Lin, Y., Guo, Z., Chen, Y., Fu, Q., Fu, J. S., and Chen,
777 J.: Probing the severe haze pollution in three typical regions of China, Atomspheric Environment,
778 10.1016/j.atmosenv.2015.08.076, 2015a.
779 Wang, T., Nie, W., Gao, J., Xue, L. K., Gao, X. M., Wang, X. F., Qiu, J., Poon, C. N., Meinardi, S., Blake, D.,
780 Wang, S. L., Ding, A. J., Chai, F. H., Zhang, Q. Z., and Wang, W. X.: Air quality during the 2008 Beijing
781 Olympics, Atmospheric Chemistry and Physics, 10.5194/acp-10-7603-2010, 2010.
782 Wang, X., Wang, W., Yang, L., Gao, X., Nie, W., Yu, Y., Xu, P., Zhou, Y., and Wang, Z.: The secondary formation
783 of inorganic aerosols in the droplet mode through heterogeneous aqueous reactions under haze conditions,
784 Atmos. Environ., 10.1016/j.atmosenv.2012.09.029, 2012.
785 Wang, Z., Li, Y., Chen, T., Li, L., Liu, B., Zhang, D., Sun, F., Wei, Q., Jiang, L., and Pan, L.: Changes in
786 atmospheric composition during the 2014APEC conference in Beijing, Journal of Geophysical Research:
787 Atmospheres, 2015b.
788 Wu, C., Huang, X. H. H., Ng, W. M., Griffith, S. M., and Yu, J. Z.: Inter-comparison of NIOSH and IMPROVE
789 protocols for OC and EC determination: implications for inter-protocol data conversion, Atmospheric
790 Measurement Techniques, 9, 4547-4560, 10.5194/amt-9-4547-2016, 2016.
791 Wu, C., and Yu, J. Z.: Determination of primary combustion source organic carbon-to-elemental carbon (OC / EC)
792 ratio using ambient OC and EC measurements: secondary OC-EC correlation minimization method,
793 Atmospheric Chemistry and Physics, 16, 5453-5465, 10.5194/acp-16-5453-2016, 2016.
794 Wu, Z., Wang, Y., Tan, T., Zhu, Y., Li, M., Shang, D., Wang, H., Lu, K., Guo, S., Zeng, L., and Zhang, Y.: Aerosol
795 Liquid Water Driven by Anthropogenic Inorganic Salts: Implying Its Key Role in Haze Formation over the
796 North China Plain, Environmental Science & Technology Letters, 5, 160-166, 10.1021/acs.estlett.8b00021,
797 2018.
798 Wyche, K. P., Ryan, A. C., Hewitt, C. N., Alfarra, M. R., McFiggans, G., Carr, T., Monks, P. S., Smallbone, K. L.,
799 Capes, G., Hamilton, J. F., Pugh, T. A. M., and MacKenzie, A. R.: Emissions of biogenic volatile organic
800 compounds and subsequent photochemical production of secondary organic aerosol in mesocosm studies of
801 temperate and tropical plant species, Atmospheric Chemistry and Physics, 14, 12781-12801,
802 10.5194/acp-14-12781-2014, 2014.
803 Xing, L., Fu, T. M., Cao, J. J., Lee, S. C., Wang, G. H., Ho, K. F., Cheng, M. C., You, C. F., and Wang, T. J.:
804 Seasonal and spatial variability of the OM/OC mass ratios and high regional correlation between oxalic acid
805 and zinc in Chinese urban organic aerosols, Atmospheric Chemistry and Physics, 13, 4307-4318, 2013.

Xu, R., Tang, G., Wang, Y., and Tie, X.: Analysis of a long-term measurement of air pollutants (2007-2011) in North China Plain (NCP); Impact of emission reduction during the Beijing Olympic Games, Chemosphere, 159, 647-658, 10.1016/j.chemosphere.2016.06.025, 2016.

Xu, W., Han, T., Du, W., Wang, Q., Chen, C., Zhao, J., Zhang, Y., Li, J., Fu, P., Wang, Z., Worsnop, D. R., and Sun, Y.: Effects of Aqueous-Phase and Photochemical Processing on Secondary Organic Aerosol Formation and Evolution in Beijing, China, Environ. Sci. Technol., 51, 762-770, 10.1021/acs.est.6b04498, 2017.

Yu, S., Zhang, Q., Yan, R., Wang, S., Li, P., Chen, B., Liu, W., and Zhang, X.: Origin of air pollution during a weekly heavy haze episode in Hangzhou, China, Environmental Chemistry Letters, 12, 543-550, 10.1007/s10311-014-0483-1, 2014.

Zheng, G. J., Duan, F. K., Su, H., Ma, Y. L., Cheng, Y., Zheng, B., Zhang, Q., Huang, T., Kimoto, T., Chang, D., Pöschl, U., Cheng, Y. F., and He, K. B.: Exploring the severe winter haze in Beijing: the impact of synoptic weather, regional transport and heterogeneous reactions, Atmospheric Chemistry and Physics, 15, 2969-2983, 10.5194/acp-15-2969-2015, 2015.

Table 1. The ratios of mean $(OC/EC)_{pri}$, SOC/OC, and POC/OC and the mass concentrations (μg m^{-3}) of OC, EC, POC, and SOC during the five stages.

Stages	$(OC/EC)_{pri}$	EC	POC	SOC	SOC/OC	POC/OC	OC/EC
S1	1.7	1.8	3.0	3.8	0.50	0.50	4.0
S2	1.8	1.4	2.4	2.2	0.41	0.59	3.6
S3	2.6	1.4	3.8	2.0	0.34	0.66	4.2
S4	1.8	1.4	2.4	1.8	0.44	0.56	4.2
S5	2.9	2.2	6.2	2.2	0.22	0.78	4.5
Mean	2.20	1.7	3.7	2.6	0.38	0.62	4.1

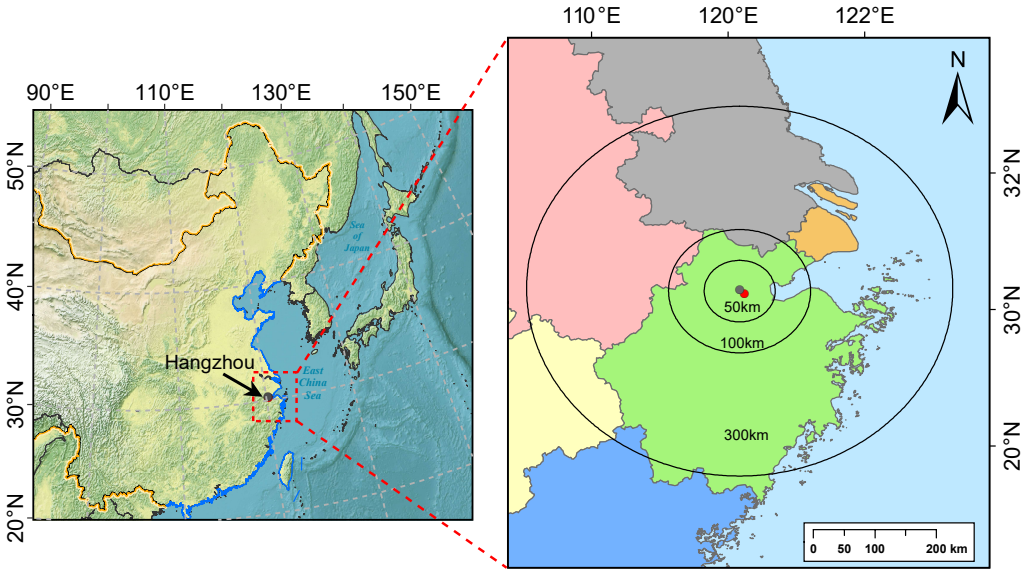

Figure 1. Geographic locations of Zhejiang (green), Shanghai (blue), Jiangsu (brown), Anhui (pink), Jiangxi (purple), and Fujian (gray) as visualized by different colors. The red dot in the right panel represents the main venue of the Hangzhou G20 Summit and the gray one denotes the location of the observational site in this study. By taking the main venue as the center of the emission control zone, three regions were set up with respect to different control intensities, i.e. the core emission control zone (r <50km), the strict emission control zone (r <100km), and the general emission control zone (r <300km).

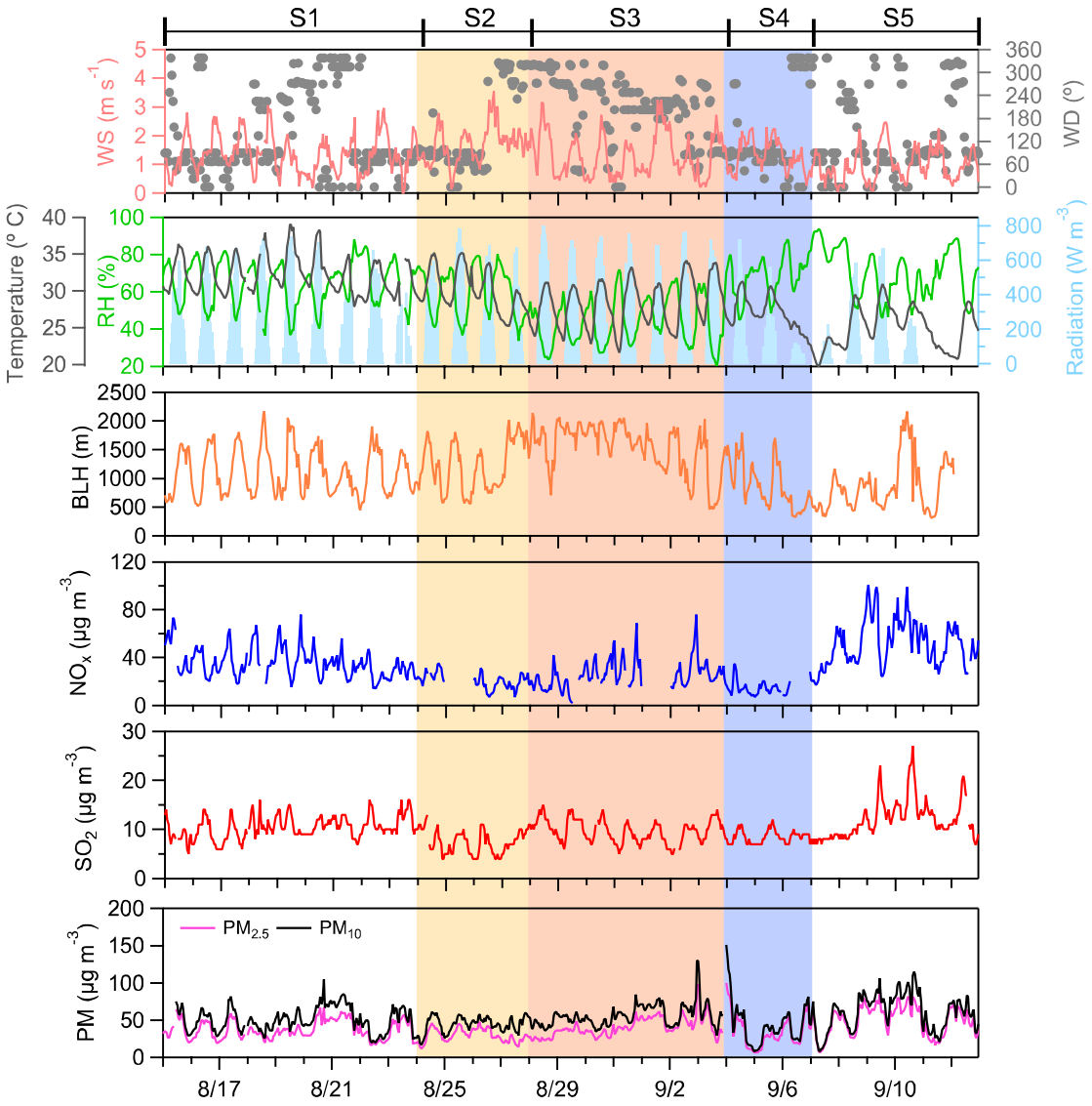

Figure 2. Time series of hourly $PM_{2.5}$ and PM_{10} concentrations, together with trace gases (NO_x, SO_2) and meteorological parameters (Wind Speed (WS), Wind Direction (WD), Boundary Layer Height (BLH), Relative humidity (RH), Temperature (T), and Radiation). The defined five stages from S1-S5 are marked on the top of the figure. S1 was the reference stage; S2 was the stage of industrial and construction emissions control; S3 added restriction on the motor vehicles; S4 was the G20 Summit period; S5 was the post-G20 stage. The missing data in Fig. 2 were due to the malfunction or maintenance of the instruments.

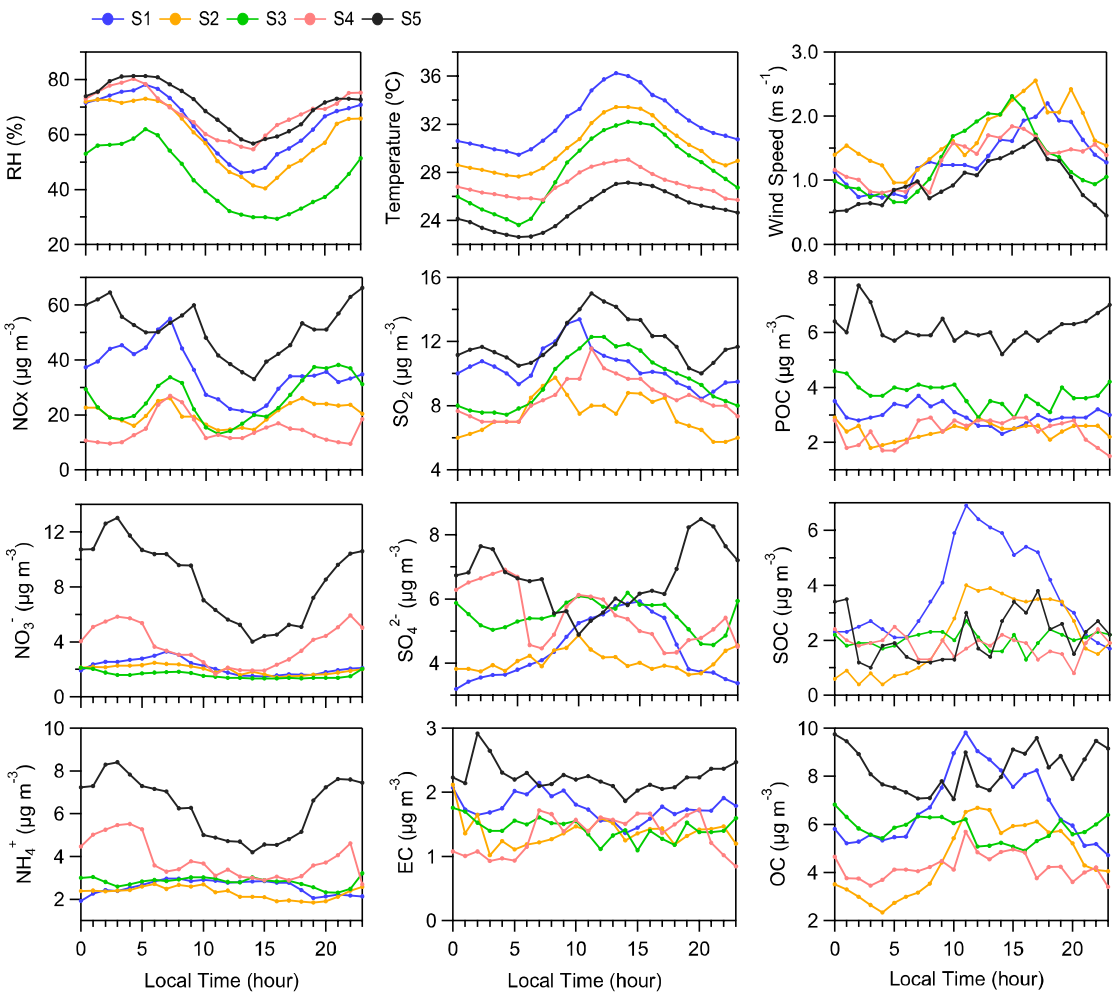

Figure. 3. Diurnal profiles of $PM_{2.5}$ species, gaseous pollutants, and meteorological variables during the five stages.

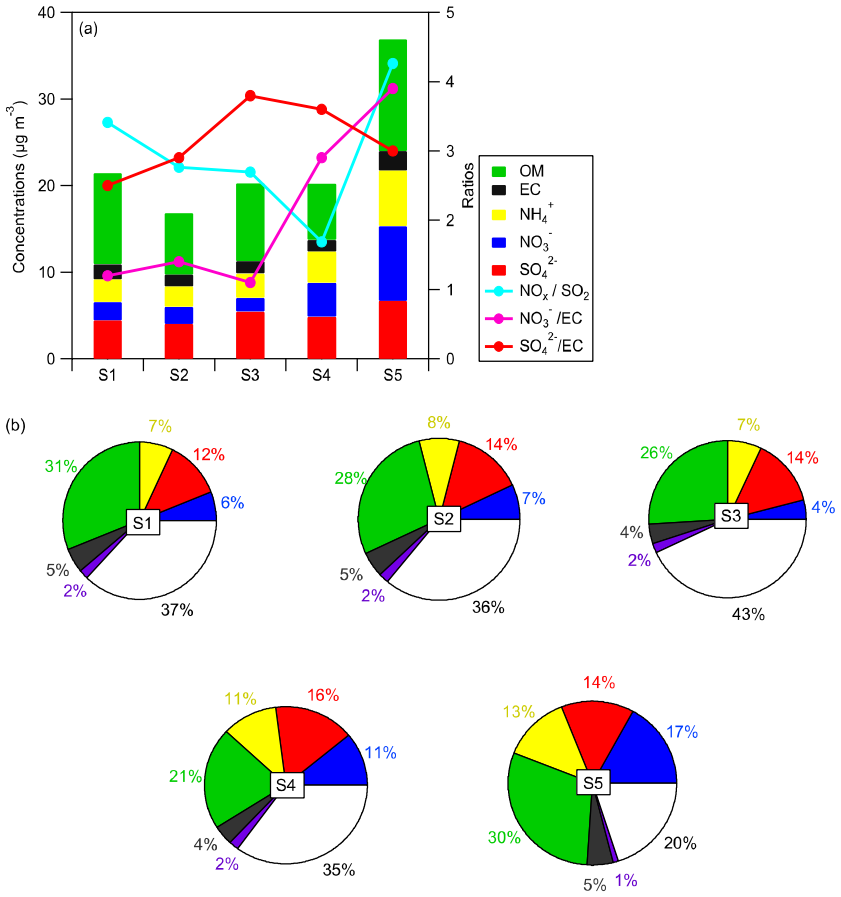

Figure 4. (a) Mean concentrations of major chemical components of $PM_{2.5}$ with respect to different stages. OM (organic matter) was estimated based on OC multiplied by a factor of 1.8 in this study (Xing et al., 2013). The mass ratios of NO_x/SO_2, NO_3^-/EC, and SO_4^{2-}/EC at each stage are also plotted. (b) Mass fractions of the measured aerosol chemical components from S1 to S5. The different color numbers for the pie chart denote the mass fractions of major aerosol constituents, i.e., green for organic matter (OM), black for elemental carbon (EC), red for SO_4^{2-}, dark blue for NO_3^-, yellow for NH_4^+, purple for the sum of Ca^{2+}, Mg^{2+}, K^+, Na^+, and Cl^-.

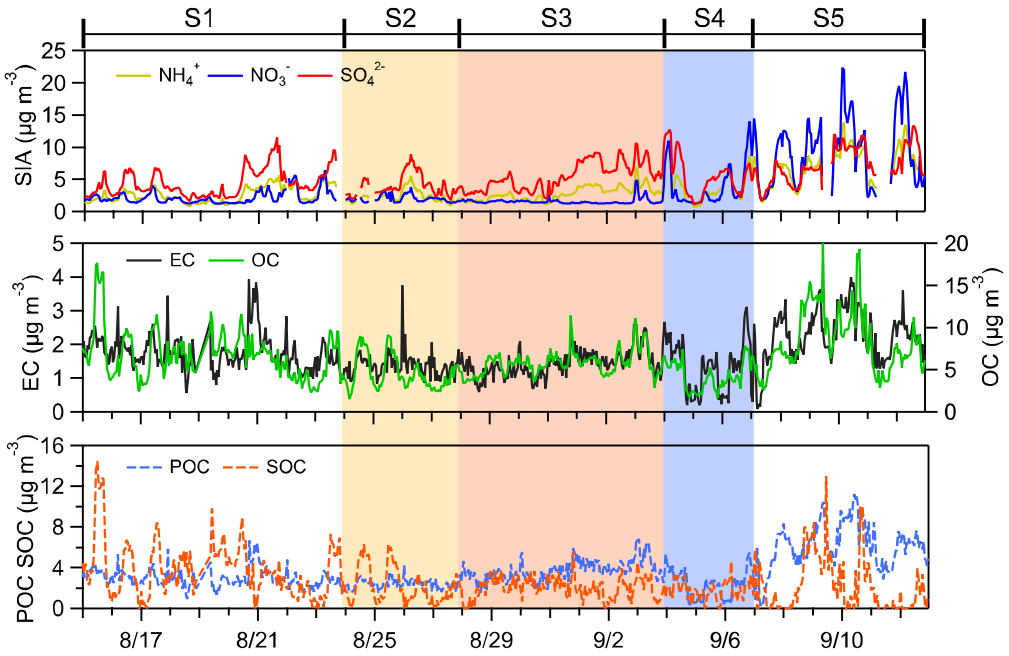

Figure 5. Time-series of $PM_{2.5}$ chemical components during the entire study period.

973

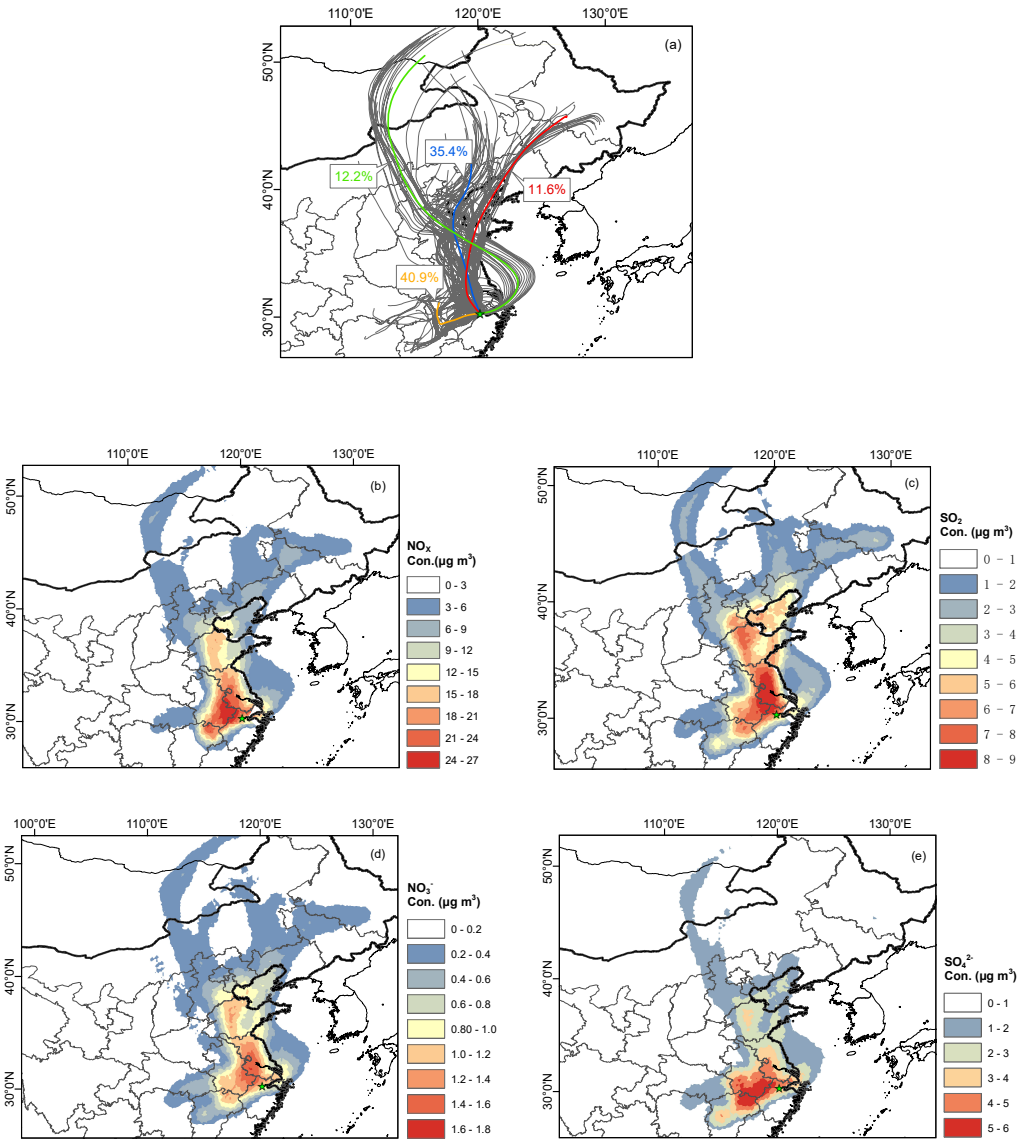

974

975 **Figure 6.** (a) Cluster analysis of the 72-h air mass backward trajectories starting at 500m in
976 Hangzhou during S3. Concentration-Weighted Trajectory (CWT) maps for (b) NO_x, (c) SO_2, (d)
977 NO_3^-, and (e) SO_4^{2-} for the whole S3 period. The location of the monitoring site is marked by a
978 green star.

979

980

981

982

983

984

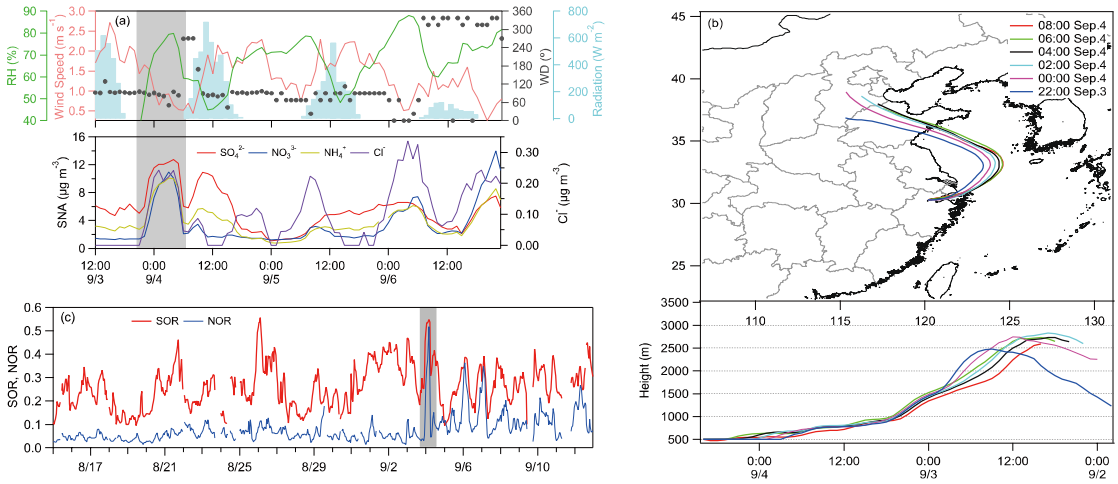

985

986

987 **Figure 7.** (a) Time series of hourly concentrations of SNA, Cl^-, and meteorological
988 parameters (WS, WD, RH, and Radiation) during S4; (b) 48-h air mass backward trajectories for
989 the short pollution episode in the morning of September 4, 2016; (c) Hourly variations of SOR and
990 NOR during the entire study period. The highlighted period represents the short pollution episode
991 in the morning of September 4, 2016.

992

993

994

995

996

997

998

999

1000

1001

1002

1003

1004

1005

1006

1007

1008

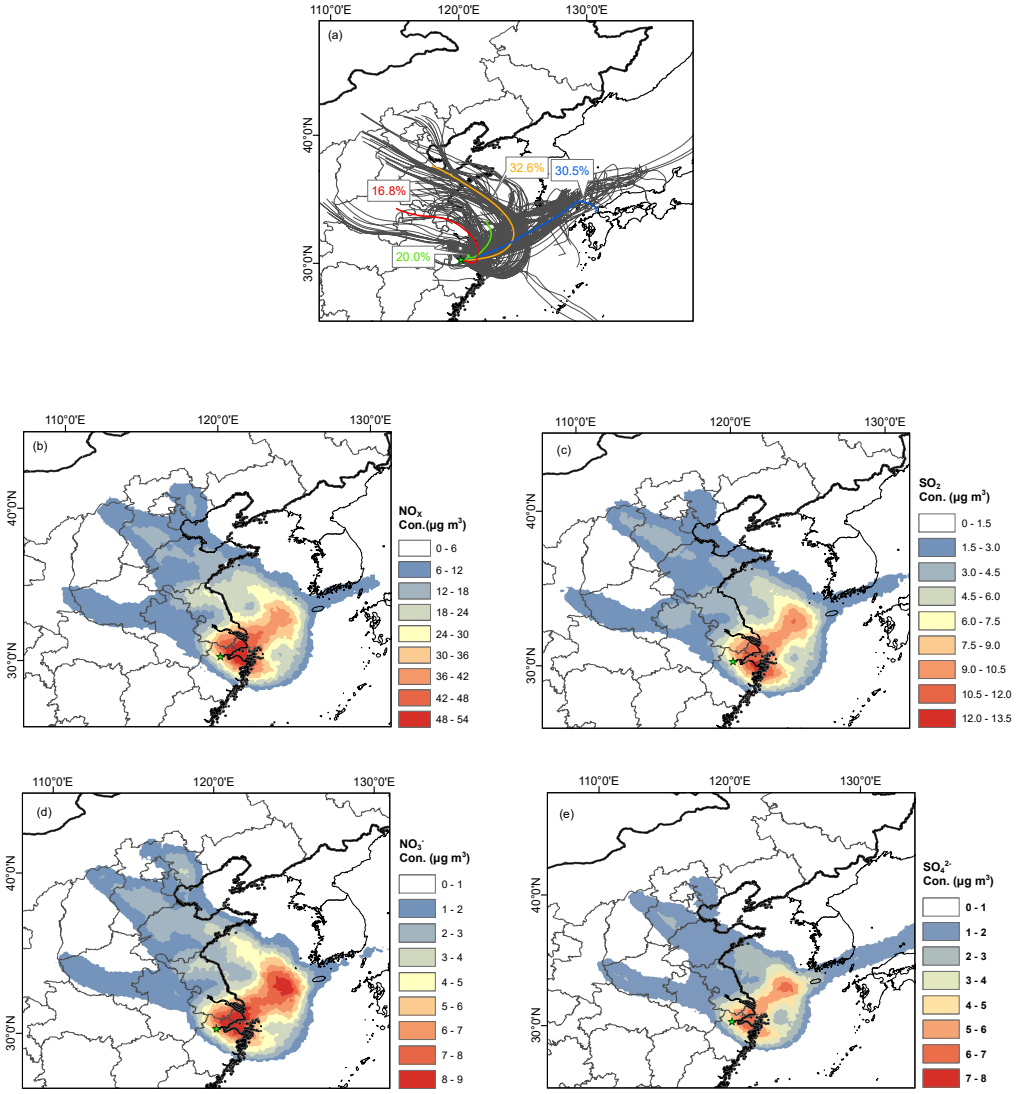

Figure 8. (a) Clustering analysis of 72-h air mass backward trajectories starting at 200m during S5. The choose of 200m is due to the low boundary layer height (about 500m on average) during this stage. Concentration-Weighted Trajectory (CWT) maps for (b) NO_x, (c) SO_2, (d) NO_3^-, and (e) SO_4^{2-} for the whole S5 period. The location of the monitoring site is marked by a green star.

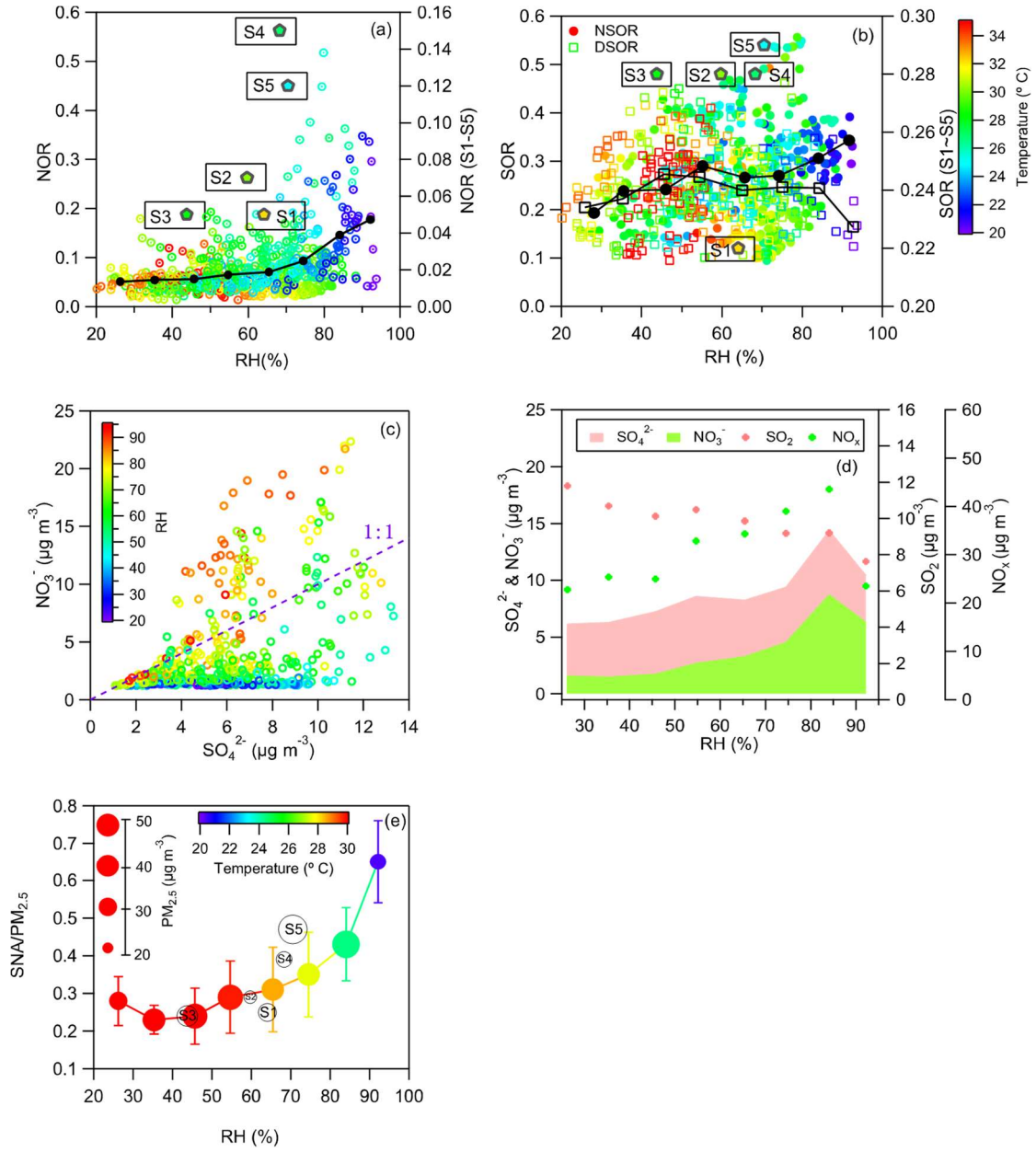

Figure 9. Hourly nitrogen oxidation ratio (NOR) (a) and sulfur oxidation ratio (SOR) (b) plotted against RH colored with temperature. The pentagons in (a) & (b) denote the mean values of NOR and SOR in each stage and the values use the right axis; DSOR and NSOR mean the SOR values during daytime and nighttime, respectively. (c) Relationship between hourly sulfate and nitrate colored by RH. (d) Hourly SO_4^{2-}, NO_3^-, SO_2, and NO_x as a function of RH. (e) The ratio of $SNA/PM_{2.5}$ as function of RH in each bin of 10%. The filled circles are colored with temperature and the sizes of the circles correspond to the mass concentrations of $PM_{2.5}$. The error bars refer to one standard deviation of the $SNA/PM_{2.5}$ values.

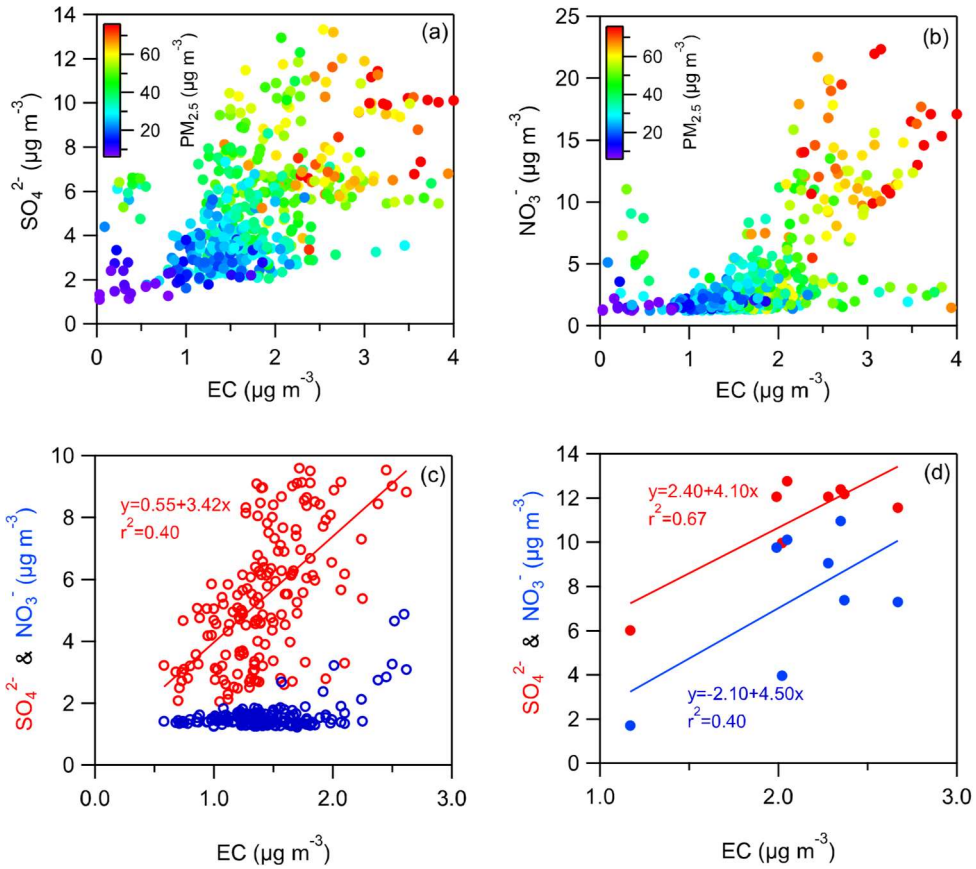

Figure 10. Hourly sulfate (a) and nitrate (b) plotted against EC colored with $PM_{2.5}$ mass concentrations. Data in Fig. 10a & 10b included the whole study period by excluding data in Fig. 10c & 10d. (c) Relationship between hourly sulfate, nitrate and EC from 0:00 AM on 28 August to 21:00 PM on 3 September. (d) Relationship between hourly sulfate, nitrate and EC from 22:00 PM on 3 September-5:00 AM LT on 4 September, respectively.

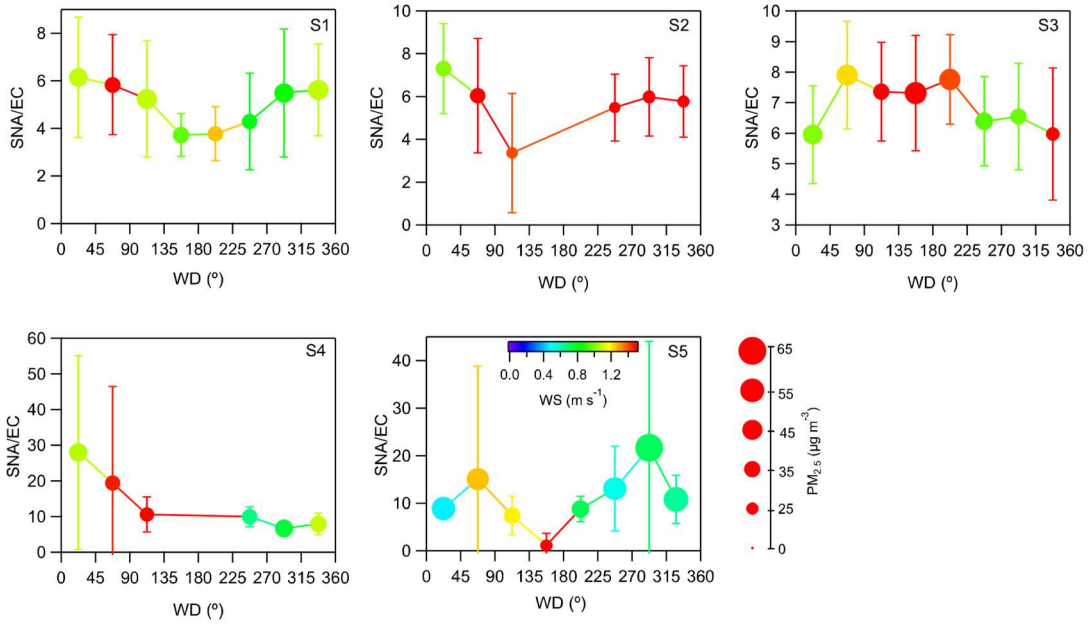

Figure 11. Variation of the ratio of SNA/$PM_{2.5}$ in eight wind direction sectors with the bin width of 45 degrees during the five stages. The filled circles are colored with wind speed and the sizes of the circles correspond to the mass concentrations of $PM_{2.5}$. The error bars refer to one standard deviation of the SNA/EC values.